1966

Double pion production without annihilation in antiproton-proton interactions at 2.7 BeV/c

Henry Bert Crawley
Iowa State University

67-5576

CRAWLEY, Henry Bert, 1940-

DOUBLE PION PRODUCTION WITHOUT ANNIHILATION IN ANTIPROTON-PROTON INTERACTIONS AT 2.7 BeV/c.

Iowa State University of Science and Technology, Ph.D., 1966
Physics, nuclear

University Microfilms, Inc., Ann Arbor, Michigan

DOUBLE PION PRODUCTION WITHOUT ANNIHILATION IN ANTIPROTON-PROTON INTERACTIONS AT 2.7 BeV/c

by

Henry Bert Crawley

A Dissertation Submitted to the
Graduate Faculty in Partial Fulfillment of
The Requirements for the Degree of
DOCTOR OF PHILOSOPHY

Major Subject: Physics

Approved:

Signature was redacted for privacy.

In Charge of Major Work

Signature was redacted for privacy.

Head of Major Department

Signature was redacted for privacy.

Dean of Graduate College

Iowa State University
Of Science and Technology
Ames, Iowa

1966

TABLE OF CONTENTS

ABSTRACT

A study was made of the reaction $\bar{p}p \rightarrow \bar{p}p\pi^+\pi^-$ at an incident antiproton momentum of 2.7 BeV/c. The total cross section for this reaction was determined to be 1.93 ± 0.16 mb. The data were found to be consistent with 100% $N^*\bar{N}^*$ formation where N^* is the pion-nucleon resonance with $T = T_z = J = 3/2$, central mass value 1238 MeV, and width 125 MeV. It was observed that the $\bar{N}^*$ production is highly peripheral; that is, in the over-all center of mass system more than 50% of the $\bar{N}^*$'s are produced with a production angle whose cosine is greater than 0.8.

A comparison of the data with the predictions of the form-factor and absorption one-pion-exchange models was made. For the form-factor model only the contribution from the "double-isobar" diagram was included, as modified by the form-factor and off-shell corrections given by Selleri. The $T_z = 1/2$ diagram was excluded because it is predicted to contribute only 1% of that of the double-isobar diagram. Finally, the contribution from the Drell diagrams was excluded on empirical grounds, since the Drell diagrams contribute to zero or single resonance production, and the data are consistent with 100% double resonance formation. For the absorption model the predictions supplied by Hite and Jackson were compared with the data. It is found that both models account for the peripherality of the $\bar{N}^*$ production and for the effective mass

ABSTRACT

A study was made of the reaction $\bar{p}p \rightarrow \bar{p}p\pi^+\pi^-$ at an incident antiproton momentum of 2.7 BeV/c. The total cross section for this reaction was determined to be 1.93 ± 0.16 mb. The data were found to be consistent with 100% $N^*\bar{N}^*$ formation where N^* is the pion-nucleon resonance with $T = T_z = J = 3/2$, central mass value 1238 MeV, and width 125 MeV. It was observed that the $\bar{N}^*$ production is highly peripheral; that is, in the over-all center of mass system more than 50% of the $\bar{N}^*$'s are produced with a production angle whose cosine is greater than 0.8.

A comparison of the data with the predictions of the form-factor and absorption one-pion-exchange models was made. For the form-factor model only the contribution from the "double-isobar" diagram was included, as modified by the form-factor and off-shell corrections given by Selleri. The $T_z = 1/2$ diagram was excluded because it is predicted to contribute only 1% of that of the double-isobar diagram. Finally, the contribution from the Drell diagrams was excluded on empirical grounds, since the Drell diagrams contribute to zero or single resonance production, and the data are consistent with 100% double resonance formation. For the absorption model the predictions supplied by Hite and Jackson were compared with the data. It is found that both models account for the peripherality of the $\bar{N}^*$ production and for the effective mass

distribution, but that neither model is successful in explaining the decay angular distributions.

I. INTRODUCTION

Presented here is an investigation of the reaction

$$\bar{p} + p \longrightarrow \bar{p} + p + \pi^+ + \pi^- \qquad (1)$$

at an incident antiproton momentum of 2.7 BeV/c. This study is based on a total of 719 events. The experiment was performed in September, 1964, at Brookhaven National Laboratory using the 20 inch hydrogen bubble chamber at the AGS. Preliminary studies of other final states in this experiment are reported elsewhere (1-4).

Double pion production without annihilation in antiproton-proton interactions has been studied over a wide range of incident antiproton momenta. Experiments have been done at 3.28 BeV/c (5) (304 events), 3.6 BeV/c (6) (455 events), 3.66 BeV/c (7) (1, 331 events), 5.7 BeV/c (8, 9) (479 and 3, 638 events), and 6.94 BeV/c (10) (155 events). All of these experiments were performed using bubble chamber techniques.

Recently, extensive use has been made of one-meson-exchange models (11) to calculate total cross sections, angular distributions, invariant mass distributions, and decay angular correlations for meson production in meson-nucleon and nucleon-nucleon interactions in the BeV range. These calculations are usually applied to reactions with three- and four-particle final states where the final state can be interpreted

as containing one or two resonances. Two of the one-meson-exchange models are the form-factor model of Ferrari and Selleri (12) and the absorption model, the present form of which is due to Sopkovich (13), Durand and Chiu (14), and Gottfried and Jackson (15, 16). The relative merits of the two approaches have been discussed in the literature (16, 17). The experimental results reported in the present paper are compared with both models.

An outline of the experimental techniques is given in Section II. The experimental results are presented in Section III, and in Section IV these experimental results are compared with the predictions of the form-factor and absorption models. Finally, Section V is a summary of the main results of the present and previous experiments on this reaction.

II. EXPERIMENTAL PROCEDURE

The Brookhaven National Laboratory's 20 inch hydrogen bubble chamber was exposed to a beam of 2.7 BeV/c antiprotons in the Yale-BNL (18) separated beam, in a collaborative experiment by groups from Iowa State University and the University of Colorado. A total of 91, 000 pictures were taken. The analysis of all strange particle reactions is being carried out in collaboration by the two groups. For the reactions not involving strange particles the University of Colorado is analyzing the two prong events, and Iowa State University is analyzing the four and six prong events.

Any contamination of the antiproton beam would be from negatively charged pi or mu mesons of the same momentum. Since all of the beam tracks, π's, μ's, and $\bar{p}$'s, have the same momentum, but different masses, the energy spectrum of electrons knocked out of the hydrogen atoms (delta-rays) are different for the three types of particles. An analysis of the energy distribution of the delta-rays was made to determine the contamination. Muons do not interact strongly so this is the only method for detecting muon contamination. However, since pions interact strongly, it is possible to detect the presence of pions from their characteristic interactions with protons, especially the elastic scattering of π^- and p. Both of these procedures yielded consistent answers that the beam was more than 99% antiprotons.

The beam flux was determined by counting the number of beam tracks entering a fiducial volume on every tenth frame of every other roll of film. Each roll contains approximately 1, 500 frames. The beam flux was found to be 11.9 beam tracks per frame.

The four prong events which were used for the study of Reaction 1 were taken from a sample of 45, 000 frames. All frames were scanned twice, and all differences in the scans were checked again to determine the correct assignment. These scans were, respectively, 94.7 and 97.0% efficient for correct identification of four prong events. All four prong events in the fiducial region were measured in approximately 18, 000 pictures. These events were measured in three views, reconstructed in space, and kinematically fitted using the program GUTS (19). An attempt was made to fit each event to all mass hypotheses for four or five particles in the final state consistent with the selection rules of the strong interactions. The following conditions were used:

1) For four-constraint cases (no missing neutral particle) the missing mass was required to be within three standard deviations of zero. The missing mass for a given mass hypothesis is defined as:

$$(MM)^2 = \left[E_0 - \left(\sum_{i=1}^{4} E_i\right)\right]^2 - \left[\vec{P}_0 - \left(\sum_{i=1}^{4} \vec{P}_i\right)\right]^2 \qquad (2)$$

where E_o and $\vec{P}_o$ are the total energy and momentum of the initial $\bar{p}p$ system, and E_i and $\vec{P}_i$ are the total energy and momentum of the i^{th} outgoing particle. If ΔMM is the standard error in the missing mass this cutoff implies that $|MM| - 3\Delta MM$ must be less than or equal to zero.

2) For one-constraint cases (one missing neutral particle) the missing mass had to be consistent with the mass of the assumed neutral particle within three standard deviations. If M_o is the mass the missing neutral particle this implies that $|MM - M_o| - 3\Delta MM$ must be less than or equal to zero.

3) The χ^2 cutoff for no missing neutrals (four-constraint class) was $\chi^2 \leq 15$.

4) The χ^2 cutoff for one missing neutral (one-constraint class) was $\chi^2 \leq 9$.

All events that had a fit to Reaction 1 were checked for consistency with the ionization of all outgoing tracks. Just as for the delta-ray energy spectrum, the ionization, or bubble density, produced by a particle of a given momentum is different for different mass particles, since the ionization varies as $\sim 1/\beta^2$. In this first sample of 18, 000 frames approximately 95% of the events which had one or more four-constraint fits to Reaction 1 satisfied the ionization check. On examination of these acceptable events it was found possible to scan the four prong events and pick out events belong-

ing to Reaction 1 by estimating the momentum and ionization of the outgoing tracks. Hence it was decided to pre-scan the four prong events in the remainder of the film to select events to be measured in the study of this reaction. This selection process reduced the total measuring time by a factor of six.

After all such selected events found in a somewhat larger fiducial volume in 43, 500 good quality pictures had been measured, a check of the selection procedure was carried out. This was accomplished by measuring all four prongs in the same increased fiducial volume in 4, 500 pictures not included in the first sample of 18, 000 pictures and checking that all acceptable fits to Reaction 1 in this second sample had been found in the special measuring procedure.

It was observed that a significant number of events which were ionization consistent only with Reaction 1 did not get kinematic fits to this final state. To explain this fact a study was made of the stretch quantities corresponding to the measured variables from those events which did obtain acceptable fits to this reaction. The stretch quantity for a given variable is defined by (Measured Value - Fitted Value)/(Error in the Measured Value). For properly assigned errors the distribution in the stretch quantity should be normally distributed about zero with approximately 68% of the events lying between -1 and +1. For the events with fits to Reaction 1 the stretch quantities for the measured momentum, azimuth, and

dip were symmetrically distributed about zero, but the distributions were too broad. This meant that the errors assigned were slightly small. Instead of changing the errors, the acceptance criteria for four-constraint fits to Reaction 1 were relaxed. In particular, the χ^2 cutoff was increased to $\leq$ 31, and the missing mass test was increased to five standard deviations. These increases more than compensated for the slightly small error assignments, but the rigid ionization criterion kept the relaxed acceptance criteria from introducing a significant background.

The final sample consists of 719 events accepted as being due to Reaction 1. Losses from non-measurable events, scanning efficiency, and poorly measured events are estimated to account for another 80 events. The χ^2 distribution for the 719 accepted events is shown in Figure 1. The slight discontinuity at $\chi^2 = 15$ is caused by the fact that all events with $\chi^2 > 15$ on the first measurement were remeasured.

A possible background reaction which could yield accidental fits to Reaction 1 while passing the ionization test is the process

$$\bar{p} + p \longrightarrow \bar{p} + p + \pi^+ + \pi^- + \pi^0 \qquad (3)$$

Despite the relaxed criteria of five standard deviations on missing mass tests, χ^2 cutoffs of $\leq$ 31 for four-constraint fits and $\leq$ 13 for one-constraint fits, no event had an ioni-

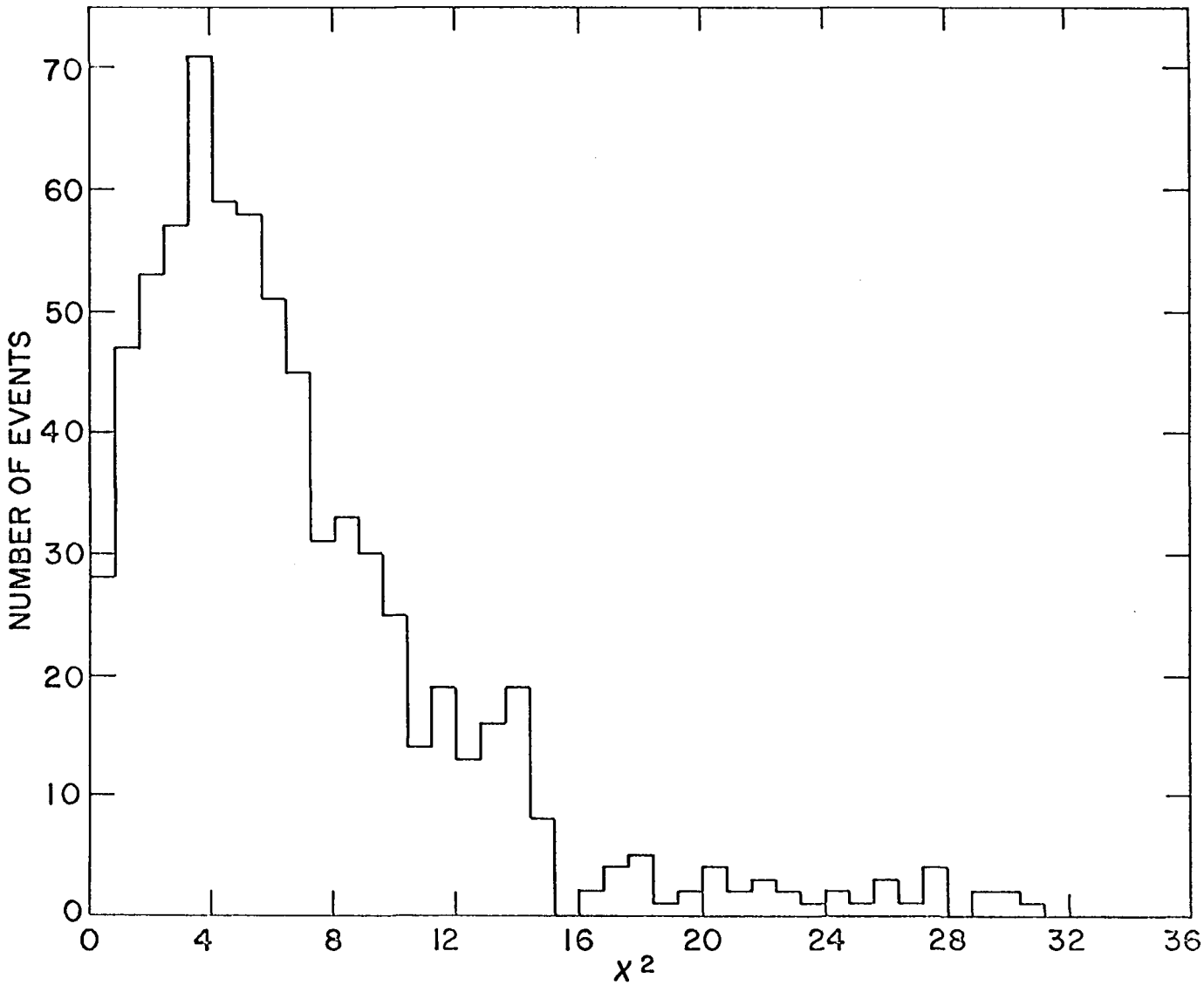

Figure 1. χ^2 distribution for the 719 accepted fits to the reaction $\bar{p}p \rightarrow \bar{p}p\pi^+\pi^-$.

zation consistent fit to both Reactions 1 and 3. Hence the sample of 719 events contains no events with consistent fits to both Reactions 1 and 3. This is due, at least in part, to the cross section for Reaction 3, which is down by a factor of twenty from that for Reaction 1.

In the center of mass system of the initial $\bar{p}$ and p the initial state is an eigenstate of CR, PR, and CP (20), where C is the charge conjugation operator, P is the parity operator, and R is a rotation of 180° about any axis perpendicular to the incident $\bar{p}$ and p line of flight. Hence the possibility of biases in the data can be examined by looking for apparent violations of C or CP invariance, since the strong interactions are invariant under these operations. The following distributions were compared for consistency with C invariance:

1) The angular distributions of the outgoing $\bar{p}$ and p with respect to the incoming $\bar{p}$ are shown in Figure 2. These distributions should be the same if one is reflected about 90°, or $\cos\theta = 0$.
2) The angular distributions of the outgoing π^- and π^+ with respect to the incoming $\bar{p}$ are shown in Figure 3 and should be compared in the same way as in 1).
3) The momentum distributions of the outgoing $\bar{p}$ and p are shown in Figure 4. These distributions should be the same.
4) The momentum distributions of the outgoing π^- and π^+

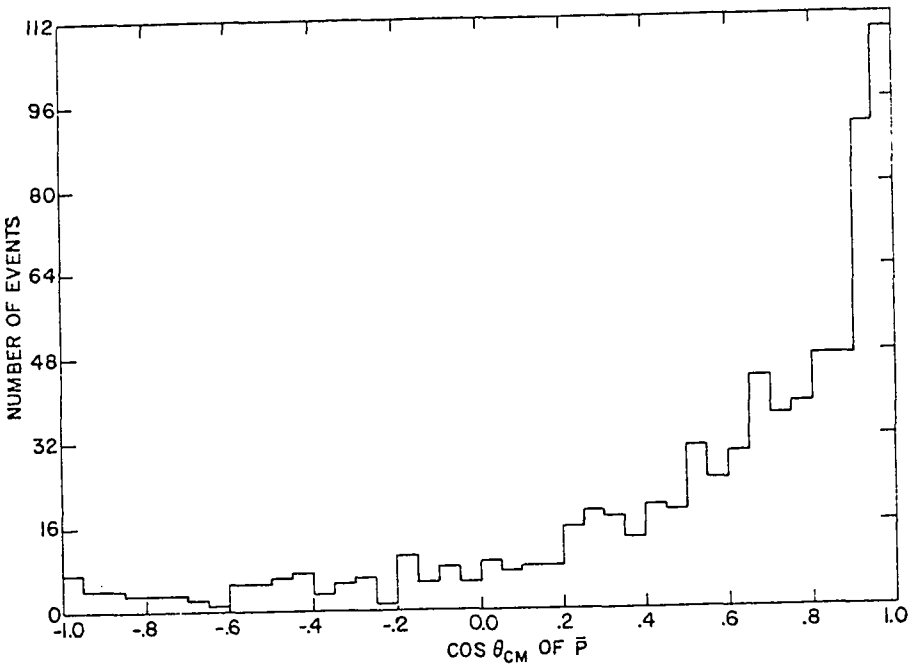

Figure 2a. Distribution of the number of events with respect to the cosine of the angle between the outgoing $\bar{p}$ and the incoming $\bar{p}$ in the over-all center of mass system for the 719 accepted fits to Reaction 1.

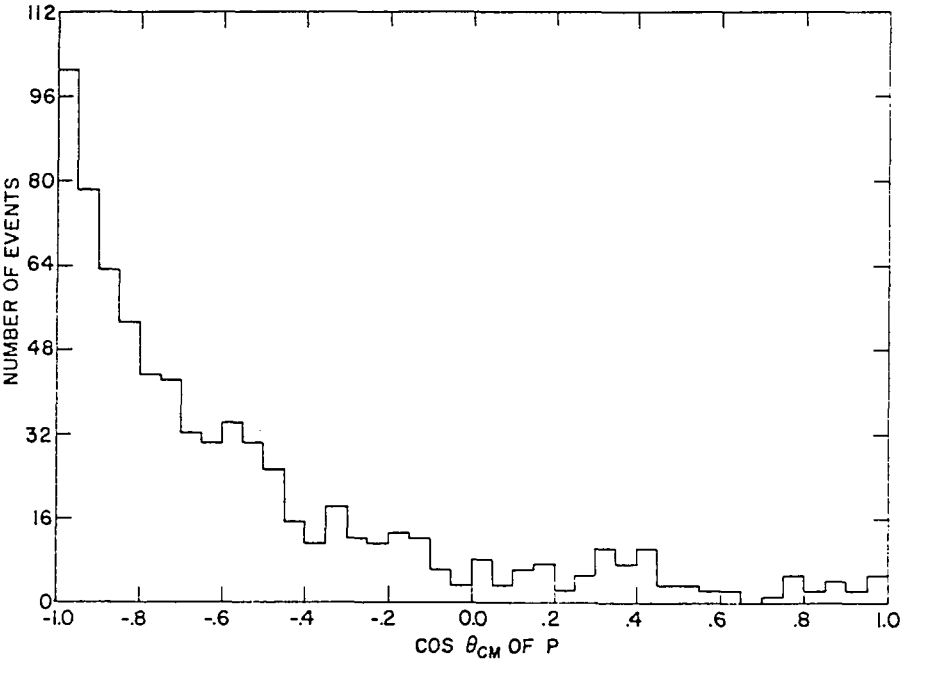

Figure 2b. Distribution of the number of events with respect to the cosine of the angle between the outgoing p and the incoming $\bar{p}$ in the over-all center of mass system for the 719 accepted fits to Reaction 1.

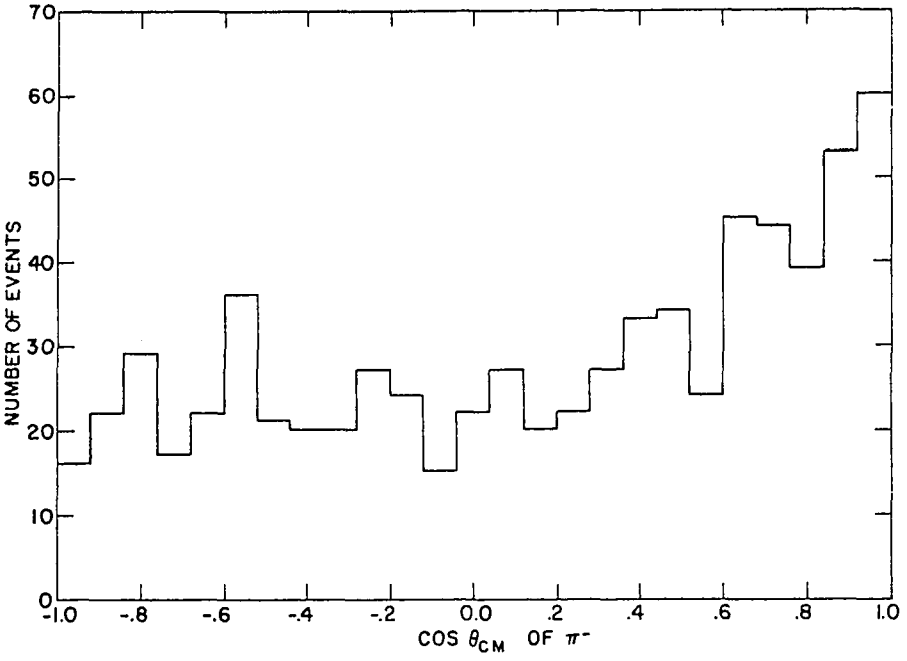

Figure 3a. Distribution of the number of events with respect to the cosine of the angle between the outgoing π^- and the incoming $\bar{p}$ in the over-all center of mass.

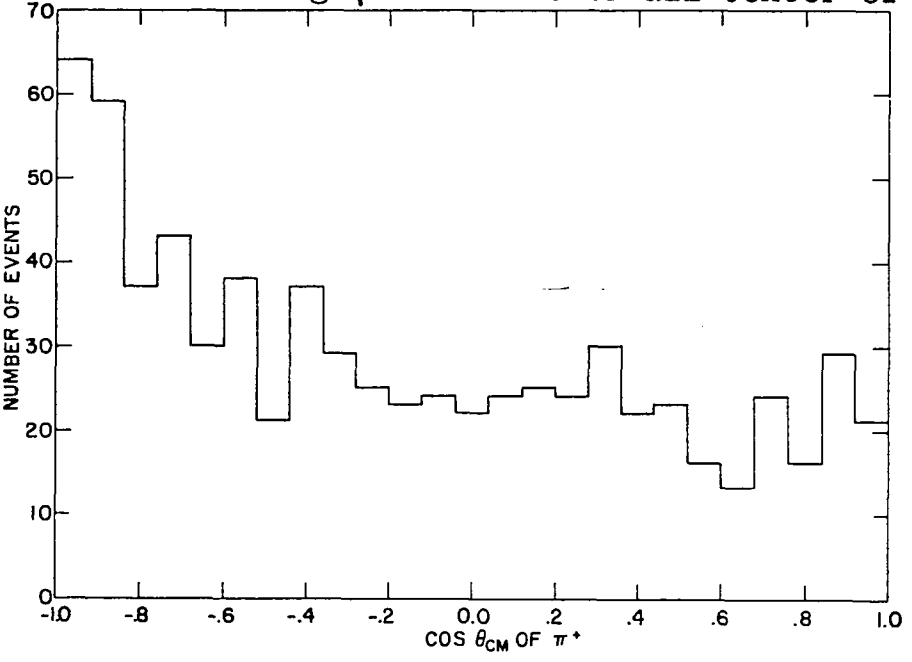

Figure 3b. Distribution of the number of events with respect to the cosine of the angle between the outgoing π^+ and the incoming $\bar{p}$ in the over-all center of mass.

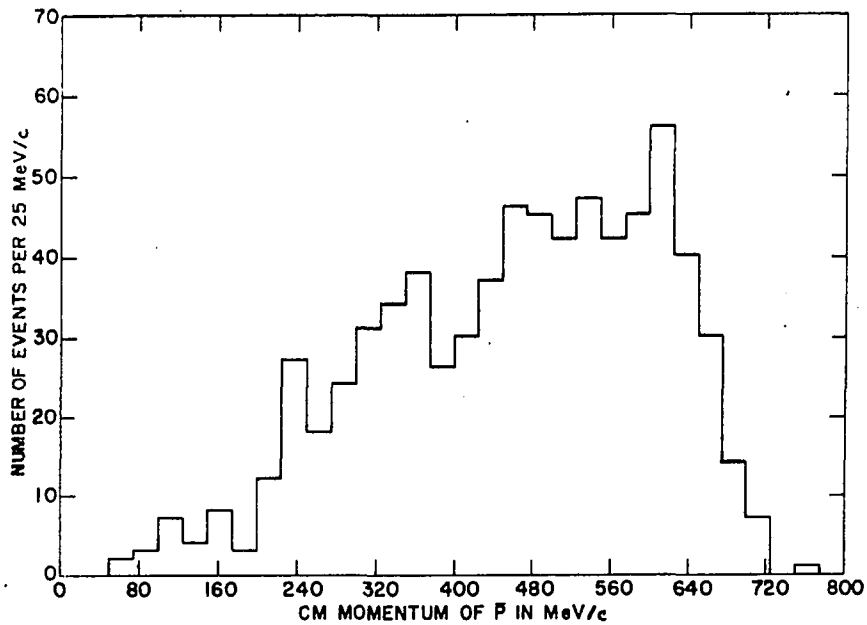

Figure 4a. Momentum distribution of the outgoing $\bar{p}$ in the over-all center of mass system for the 719 accepted fits to Reaction 1.

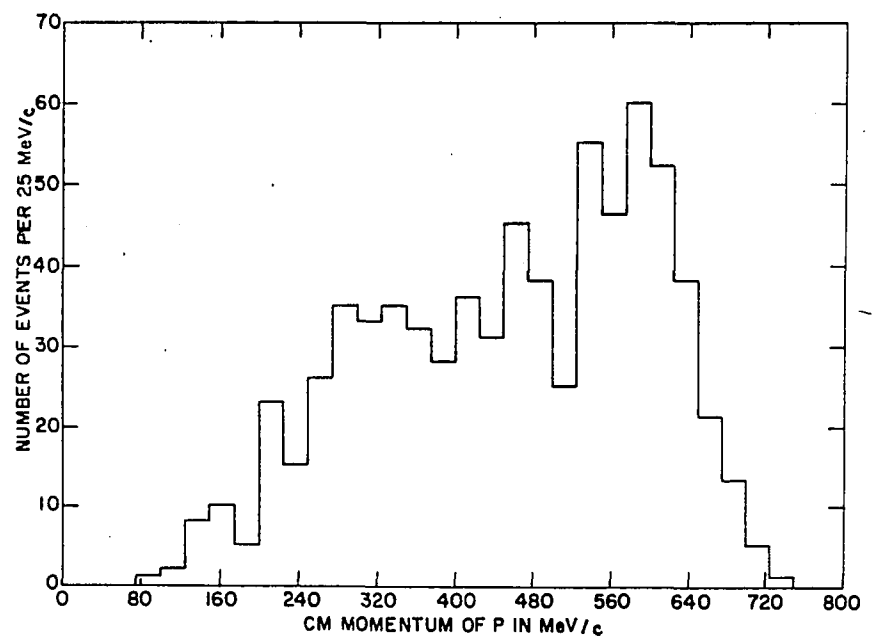

Figure 4b. Momentum distribution of the outgoing p in the over-all center of mass system for the 719 accepted fits to Reaction 1.

are shown in Figure 5, which should be the same. Departures from these requirements of C invariance are within the allowed statistical fluctuation. A further test of C and CP invariance is shown in Figure 6. The distribution of the number of events with respect to the angle between the projections of the final π^+ and p momenta onto the plane normal to the incident $\bar{p}$ momentum (in the center of mass system) is shown in Figure 6a. The corresponding distribution for the final π^- and $\bar{p}$ is shown in Figure 6b. CP invariance requires the distributions to be identical, and the addition of C invariance further requires them to be symmetric about 180°. Within statistics these requirements are satisfied.

The requirement of C invariance is used throughout Section III and Section IV. Distributions which are required by C invariance to be the same are combined when it is convenient to do so, that is, the effective mass distributions and decay angular distributions for the N* and $\bar{N}$* are combined.

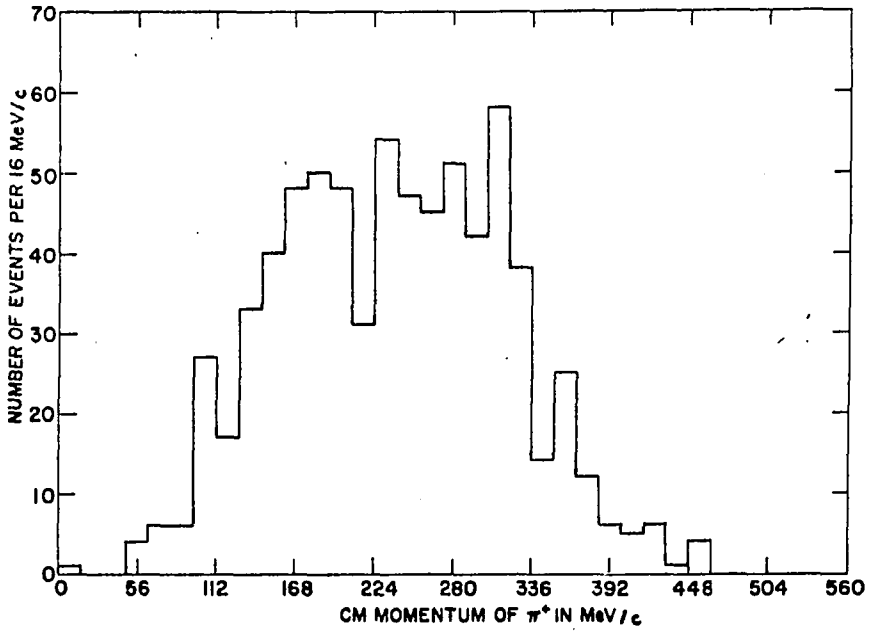

Figure 5a. Momentum distribution of the outgoing π^+ in the over-all center of mass system for the 719 accepted fits to Reaction 1.

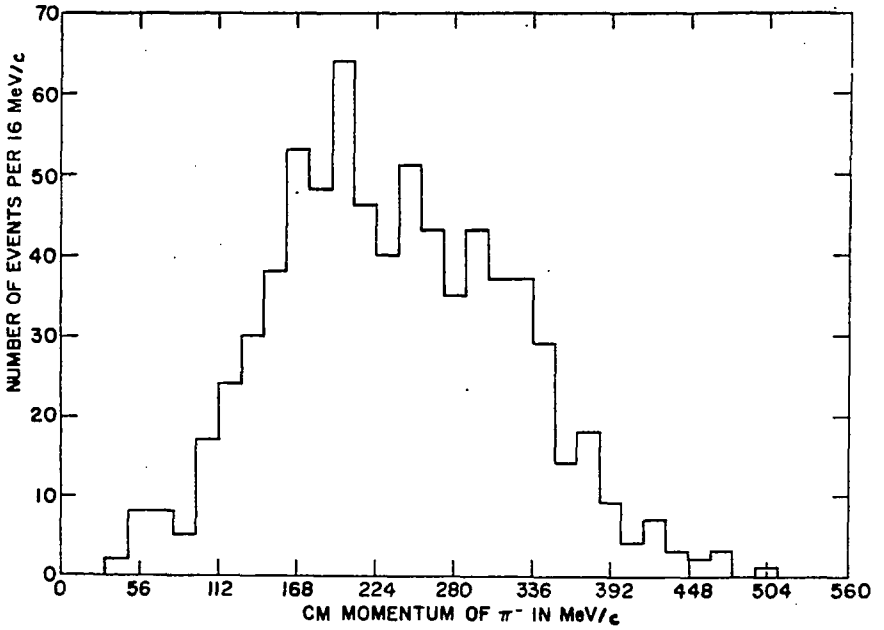

Figure 5b. Momentum distribution of the outgoing π^- in the over-all center of mass system for the 719 accepted fits to Reaction 1.

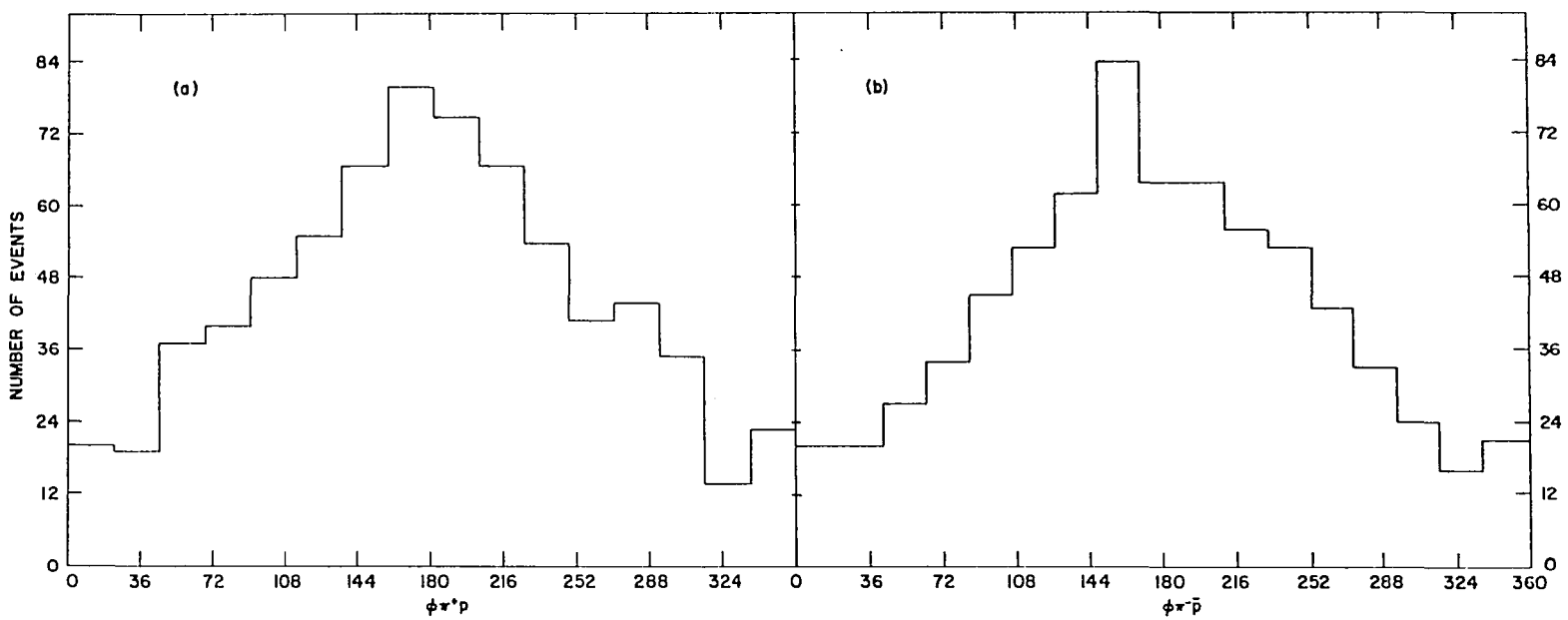

Figure 6. a) Distribution of the number of events with respect to the angle between the projections of the final π^+ and p momenta onto the plane normal to the incident $\bar{p}$ momentum (in the center of mass system). b) the same distribution for the final π^- and $\bar{p}$.

III. EXPERIMENTAL RESULTS

The total cross section for Reaction 1 is given by

$$\sigma_{Total} = \frac{\text{Number of Reaction 1 events}}{(\text{Total number of frames})(\text{Average beam tracks/frame})} \times \frac{A}{\ell \rho N_o} \qquad (4)$$

where

Number of Reaction 1 events = 799

Total number of frames = 43, 553

Average beam tracks/frame = 11.9

A = atomic weight of hydrogen = 1.008

ℓ = average length of beam tracks in the fiducial volume = 20.99 cm

ρ = density of hydrogen at 25.2° K = 0.0637 gm/cm^3

N_o = Avagodro's number = 6.025×10^{23} atoms/gram atomic weight

The number of events from Reaction 1 was taken as the number of events with accepted fits plus the number of events which were counted as losses in Section II. The average length of the beam tracks was determined from a distribution of the vertex positions of the 719 accepted fits. In evaluating the error in σ_{Total} the only significant errors are the statistical error in the number of events from Reaction 1 that were found, which is $\pm \sqrt{719}$ events, and the uncertainty in the losses, which was estimated to be $\pm$ 60 events. With these values the total cross section for Reaction 1 was found

to be $\sigma_{Total} = 1.93 \pm 0.16$ mb.

The reaction was found to proceed primarily through $N^*\bar{N}^*$ production. The dominance of double resonance production is seen in Figure 7, a two dimensional plot of the invariant mass of the combinations π^+p and $\pi^-\bar{p}$ in the final state. If E_i is the total energy and $\vec{P}_i$ is the momentum of the i^{th} particle then the square of the effective (invariant) mass of a combination of N particles is defined by

$$M^2_{1\cdots N} = \left(\sum_{i=1}^{N} E_i\right)^2 - \left(\sum_{i=1}^{N} \vec{P}_i\right)^2 .$$

The theoretical expression for the π^+p ($\pi^-\bar{p}$) invariant mass distribution was written as

$$L(\omega, \bar{\omega}) = \alpha_{\pi^+p\,\pi^-\bar{p}} F_{\pi^+p\,\pi^-\bar{p}} + \alpha_{N^*\pi^-\bar{p}} F_{N^*\pi^-\bar{p}} + \alpha_{\pi^+p\bar{N}^*} F_{\pi^+p\bar{N}^*} + \alpha_{N^*\bar{N}^*} F_{N^*\bar{N}^*} \qquad (5)$$

This expression contains phenomenological forms for the invariant mass distributions corresponding to zero resonance production ($F_{\pi^+p\,\pi^-\bar{p}}$), to single resonance production ($F_{N^*\pi^-\bar{p}}$ and $F_{\pi^+p\,\bar{N}^*}$), and to double resonance production ($F_{N^*\bar{N}^*}$) which are products of phase space factors and Breit-Wigner expressions. These F's are (21)

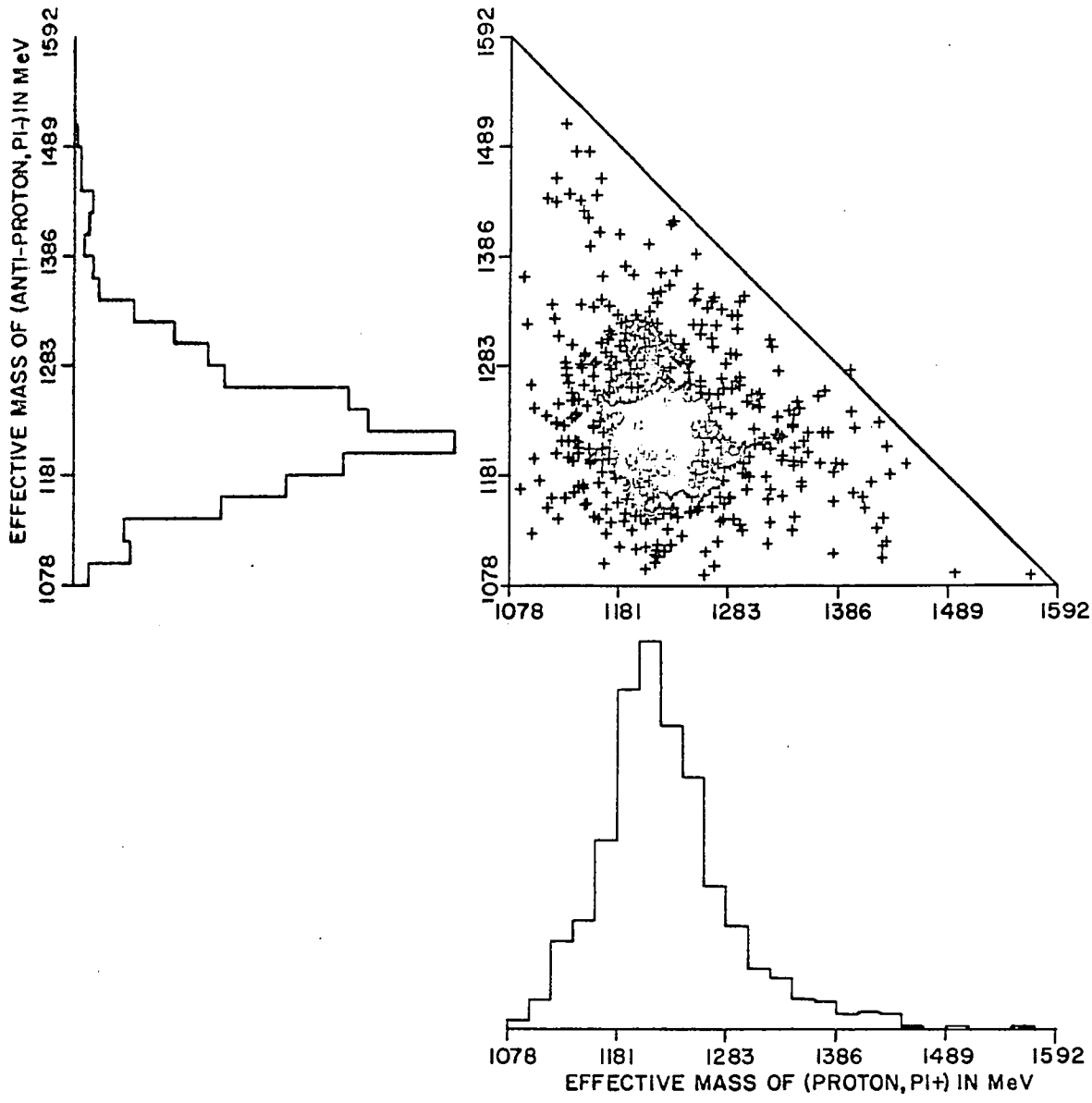

Figure 7. Two dimensional distribution of the effective masses of the final π^+p and $\pi^-\bar{p}$ combinations. The individual effective mass distributions of the π^+p and $\pi^-\bar{p}$ systems are shown as projections. The figure is based on 719 events and each event occurs once.

$$F_{\pi^+ p \pi^- \bar{p}} = C_1 \frac{P(\omega; M^2, m^2)}{\omega} \frac{P(\bar{\omega}; M^2, m^2)}{\bar{\omega}} \frac{P(E; \omega^2, \bar{\omega}^2)}{E} \omega \bar{\omega}$$

$$F_{N^* \pi^- \bar{p}} = C_2 F_{\pi^+ p \pi^- \bar{p}} \varphi(\omega)$$

$$F_{\pi^+ p \bar{N}^*} = C_3 F_{\pi^+ p \pi^- \bar{p}} \varphi(\bar{\omega})$$

$$F_{N^* \bar{N}^*} = C_4 F_{\pi^+ p \pi^- \bar{p}} \varphi(\omega) \varphi(\bar{\omega})$$

where the C's are the normalization constants, ω ($\bar{\omega}$) is the effective mass of the final $\pi^+ p$ ($\pi^- \bar{p}$) combination, $M(m)$ is the nucleon (pion) mass, and E is the total energy in the over-all center of mass system. $P(\omega; M^2, m^2)$ is the magnitude of the π^+ three-momentum in the $\pi^+ p$ rest frame

$$P(\omega; M^2, m^2) = \frac{1}{2\omega} \left[\omega^4 - 2\omega^2 (M^2 + m^2) + (M^2 - m^2)^2 \right]^{1/2}$$

$\varphi(\omega)$ is defined by

$$\varphi(\omega) = \frac{\omega}{P(\omega; M^2, m^2)} \quad \frac{\Gamma(\omega)}{(\omega^2 - \omega_0^2)^2 - \omega_0^2 \Gamma^2(\omega)}$$

where

$$\Gamma(\omega) = \Gamma_0 \left\{ \frac{P(\omega; M^2, m^2)}{P(\omega_0; M^2, m^2)} \right\}^3 \left[\frac{2.2\, m^2 + \{ P(\omega_0; M^2, m^2) \}^2}{2.2\, m^2 + \{ P(\omega; M^2, m^2) \}^2} \right]$$

The quantity in square brackets is an empirical correction to the P-wave resonance width, ω_0 is the central value of the mass of the resonance, and Γ_0 is the width parameter. Finally, the α's are the fractions of the events of the type indicated by the subscripts.

The invariant mass distribution of Figure 7 was fitted to Expression 5 by a maximum likelihood calculation (see Appendix A) using the general fitting program MINFUN (22). The C's were chosen such that each of the distributions was normalized to one so that the α's were required to sum to unity. Charge conjugation invariance requires $\alpha_{N^+\pi^-\bar{p}}$ to be equal to $\alpha_{\pi^+ p \bar{N}^+}$. In addition to the α's, ω_0 and Γ_0 were also allowed to vary in the fitting, which gave a total of four free parameters. Allowing ω_0 and Γ_0 to vary meant that the normalization constants had to be recalculated for each variation of either of these parameters.

The result of the maximum likelihood calculation is $\alpha_{\pi^+p\pi^-\bar{p}} = 0.07 \pm 0.01$, $\alpha_{N^*\pi^-\bar{p}} = \alpha_{\pi^+p\bar{N}^*} = 0.0 \pm 0.02$, $\alpha_{N^*\bar{N}^*} = 0.93 \pm 0.01$, $\omega_o = 1223.0 \pm 0.3$ MeV, and $\Gamma_o = 123.2 \pm 1.6$ MeV. This value of ω_o results in a predicted peak slightly below the observed peak in the invariant mass distribution, but does give a better over-all fit to the distribution. The errors quoted are purely statistical and do not reflect uncertainties in the forms used for the invariant mass distributions in Expression 5, that is, in the F's. In particular, fits were made restricting ω_o to a value consistent with the peak of the experimental distribution. Further, S-wave Breit-Wigner forms were tried in addition to the P-wave forms. These variations made in the forms of the F's result in $0.90 \leq \alpha_{N^*\bar{N}^*} \leq 1.00$ and $0.0 \leq \alpha_{N^*\pi^-\bar{p}} + \alpha_{\pi^+p\bar{N}^*} + \alpha_{\pi^+p\pi^-\bar{p}} \leq 0.10$. On this evidence the best estimate for the fraction of double resonance production is $\alpha_{N^*\bar{N}^*} = 0.95 \pm 0.05$. In the remainder of this paper this result is considered to be consistent with 100% double resonance production.

No N* resonances with $T_z = 1/2$ were found. Figure 8, which is a two dimensional plot of the π^-p and $\pi^+\bar{p}$ invariant masses, shows no enhancement near 1238 MeV. The N*(1518) is close to the kinematic limit of 1590 MeV and is not observed.

Of the ten possible effective mass combinations the remaining six are shown in Figure 9. There is no evidence of ρ production in the $\pi^+\pi^-$ effective mass distribution shown

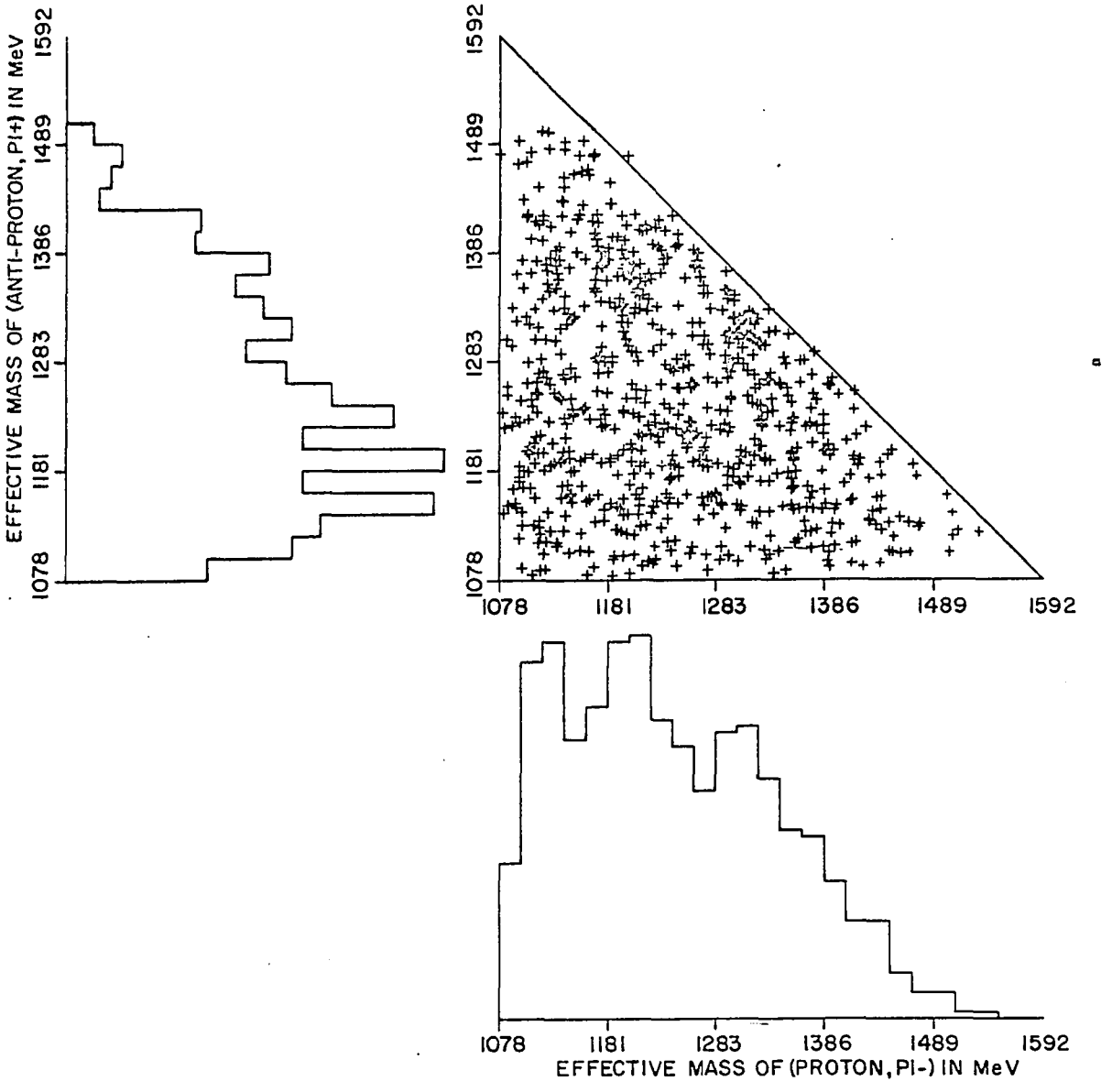

Figure 8. Two dimensional distribution of the effective masses of the final π^-p and $\pi^+\bar{p}$ combinations. The individual effective mass distributions of the π^-p and $\pi^+\bar{p}$ systems are shown as projections. The figure is based on 719 events and each event occurs once.

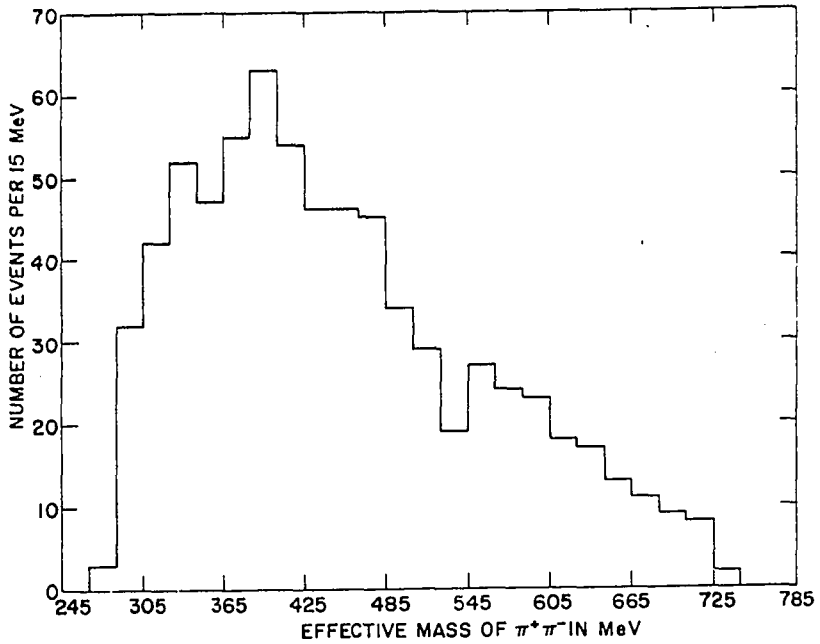

Figure 9a. Distribution of the number of events with respect to the effective mass of the $\pi^+\pi^-$ combination for the 719 accepted fits to Reaction 1.

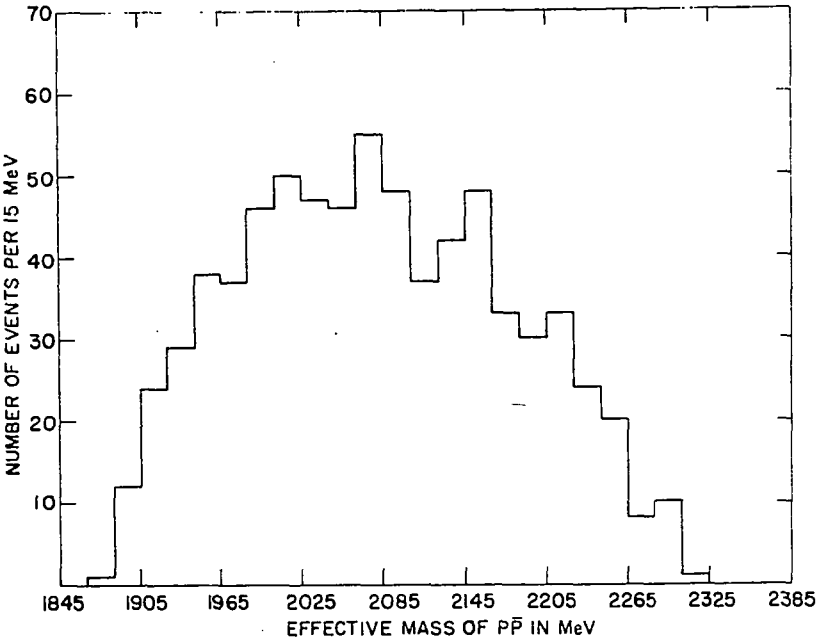

Figure 9b. Distribution of the number of events with respect to the effective mass of the $p\bar{p}$ combination for the 719 accepted fits to Reaction 1.

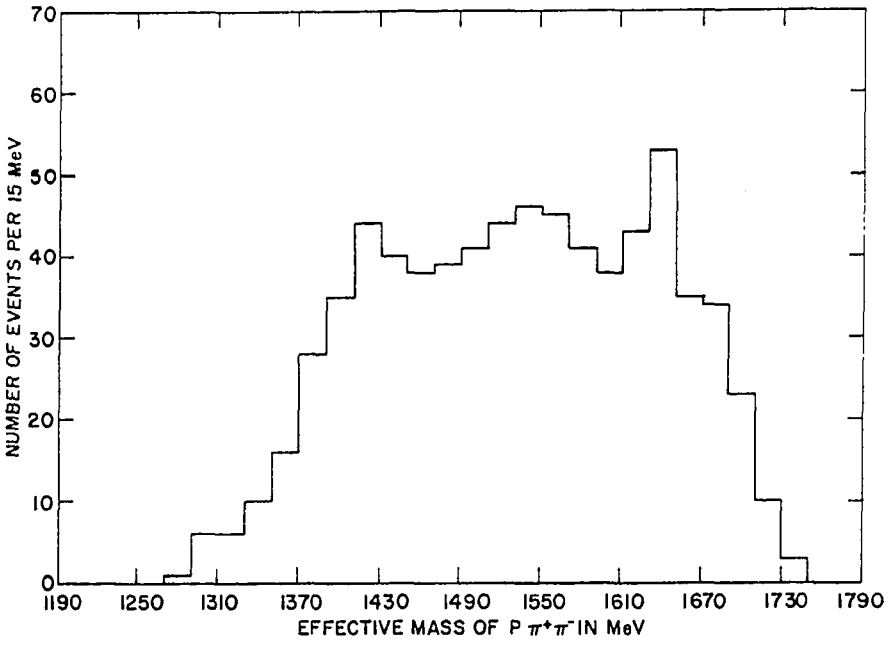

Figure 9c. Distribution of the number of events with respect to the effective mass of the $p\pi^+\pi^-$ combination for the 719 accepted fits to Reaction 1.

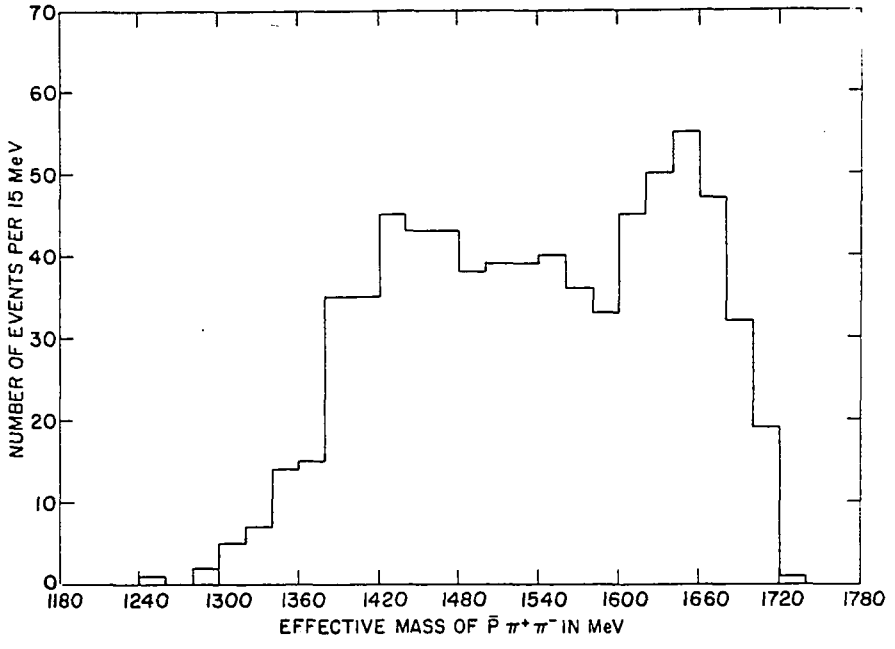

Figure 9d. Distribution of the number of events with respect to the effective mass of the $\bar{p}\pi^+\pi^-$ combination for the 719 accepted fits to Reaction 1.

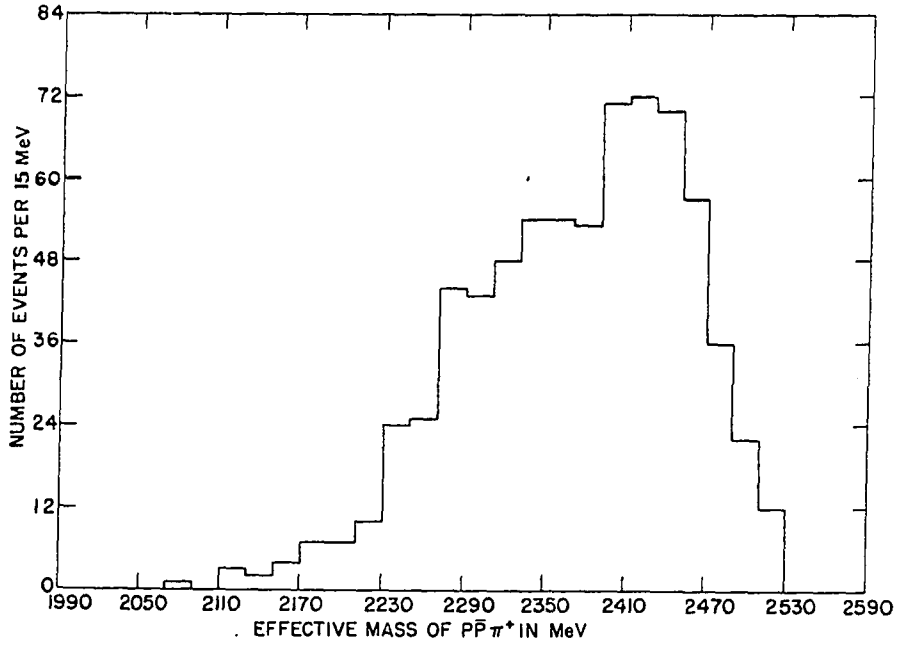

Figure 9e. Distribution of the number of events with respect to the effective mass of the $p\bar{p}\pi^+$ combination for the 719 accepted fits to Reaction 1.

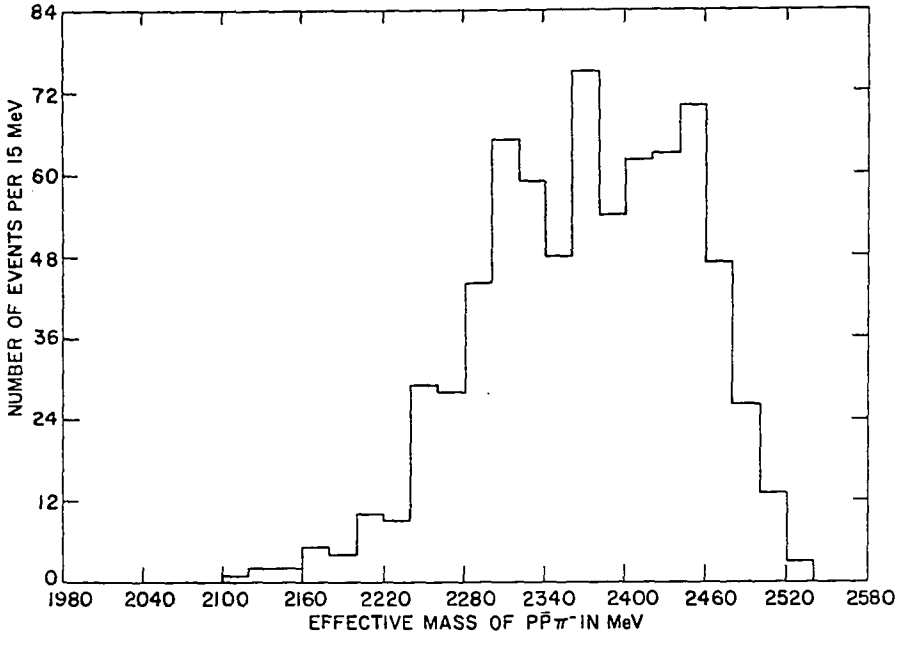

Figure 9f. Distribution of the number of events with respect to the effective mass of the $p\bar{p}\pi^-$ combination for the 719 accepted fits to Reaction 1.

in Figure 9a. The ρ mass (769 MeV) lies very close to the kinematic limit of 790 MeV. In the $p\pi^+\pi^-$ and $\bar{p}\pi^+\pi^-$ mass distributions shown in Figure 9c and 9d no enhancements were seen in the regions of the N*(1518) or N*(1688). No structure is expected in the invariant mass distributions of the combinations $p\bar{p}$ (Figure 9b), $p\bar{p}\pi^+$ (Figure 9e), or $p\bar{p}\pi^-$ (Figure 9f).

The distribution with respect to the cosine of the center of mass production angle is shown in Figure 10. The production angle θ_p is defined as the angle between the incoming $\bar{p}$ momentum and the momentum of the outgoing $\pi^-\bar{p}$ system. Of the 719 events 51% occur with $\cos\theta_p > 0.8$, that is, the angular distribution of the $\bar{N}^*$ is strongly peaked in the forward direction.

The general form for the angular distribution of the N* decay products (πN) in the N* rest frame is (23)

$$W(\theta,\varphi) = C\left\{\left(\tfrac{1}{2}-\rho_{1,1}\right)\sin^2\theta + \rho_{1,1}\left(\tfrac{1}{3}+\cos^2\theta\right)\right.$$

$$\left. -\frac{2}{\sqrt{3}}\,\mathrm{Re}\,\rho_{3,-1}\sin^2\theta\cos 2\varphi - \frac{2}{\sqrt{3}}\,\mathrm{Re}\,\rho_{3,1}\sin 2\theta\cos\varphi\right\} \quad (6)$$

The decay angles θ and φ are defined in Figure 11, and C is a normalization constant. The density matrix elements $\rho_{2m,2m'}$ are products of amplitudes for producing the N* with spin projections m and m' along the z axis, and in general may be functions of the dynamical invariants of the

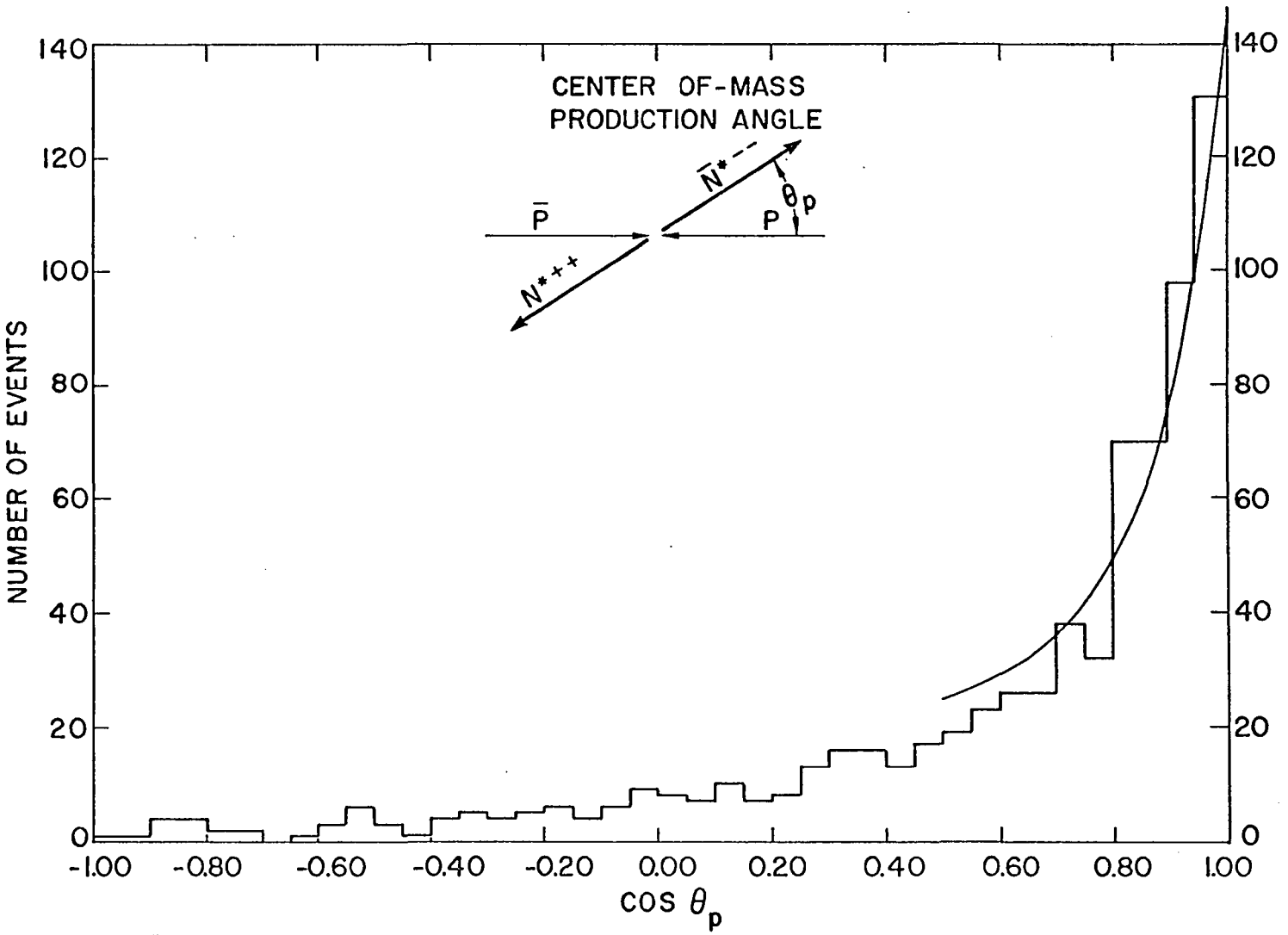

Figure 10. Differential cross section with respect to the cosine of the angle between the incoming $\bar{p}$ momentum and the momentum of the outgoing $\pi^-\bar{p}$ system in the center of mass frame. The solid curve is the absorption model prediction normalized to the number of events (533) in the region $0.5 \leq \cos\theta_p \leq 1.0$. The figure is based on 719 events.

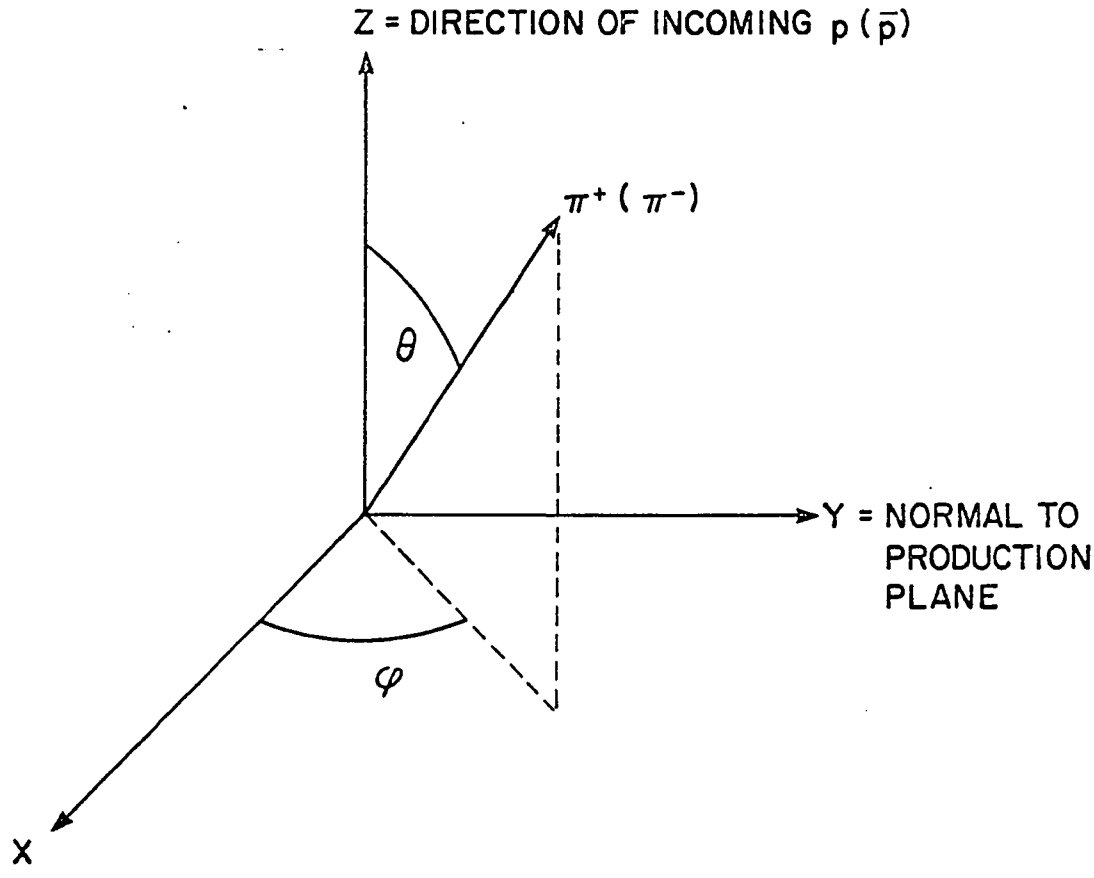

Figure 11. Definition of the decay angles θ and φ used in Equations 6-9. All directions are defined in the rest frame of the $N^*(\bar{N}^*)$.

interaction. Expression 6 is the most general form allowed for the decay of a spin 3/2 particle into a spin 1/2 baryon and spin 0 meson. The individual θ and φ distributions are obtained from Expression 6 by integration over φ and θ, respectively

$$W_1(\theta) = C_1 \left\{ \left(\tfrac{3}{4} - \rho_{1,1}\right) + 3\left(\rho_{1,1} - \tfrac{1}{4}\right) \cos^2\theta \right\} \qquad (7)$$

$$W_2(\varphi) = C_2 \left\{ 1 - \tfrac{4}{\sqrt{3}} \, \mathrm{Re}\,\rho_{3,-1} \cos 2\varphi \right\} \qquad (8)$$

where, again, C_1 and C_2 are normalization constants.

The density matrix elements $\rho_{1,1}$, Re $\rho_{3,-1}$, and Re $\rho_{3,1}$ (averaged over the production angle) were determined by a maximum likelihood calculation using Expression 4 and the combined N* and $\bar{N}$* decay data. The result is $\rho_{1,1} = 0.350 \pm 0.015$, Re $\rho_{3,-1} = -0.048 \pm 0.013$, and Re $\rho_{3,1} = 0.039 \pm 0.015$ (see Appendix B). Curves obtained using these values in Equations 7 and 8 are shown with the data in Figure 12. The distribution of the azimuthal decay angle φ, Figure 12b, shows a definite departure from isotropy. The density matrix elements as functions of the cosine of the center of mass production angle θ_p were calculated using maximum likelihood techniques and the results are shown in Figure 13. The intervals in cos θ_p over which the ρ's are averaged are indicated by the horizontal error flags.

As a further check of the consistency of the data, density

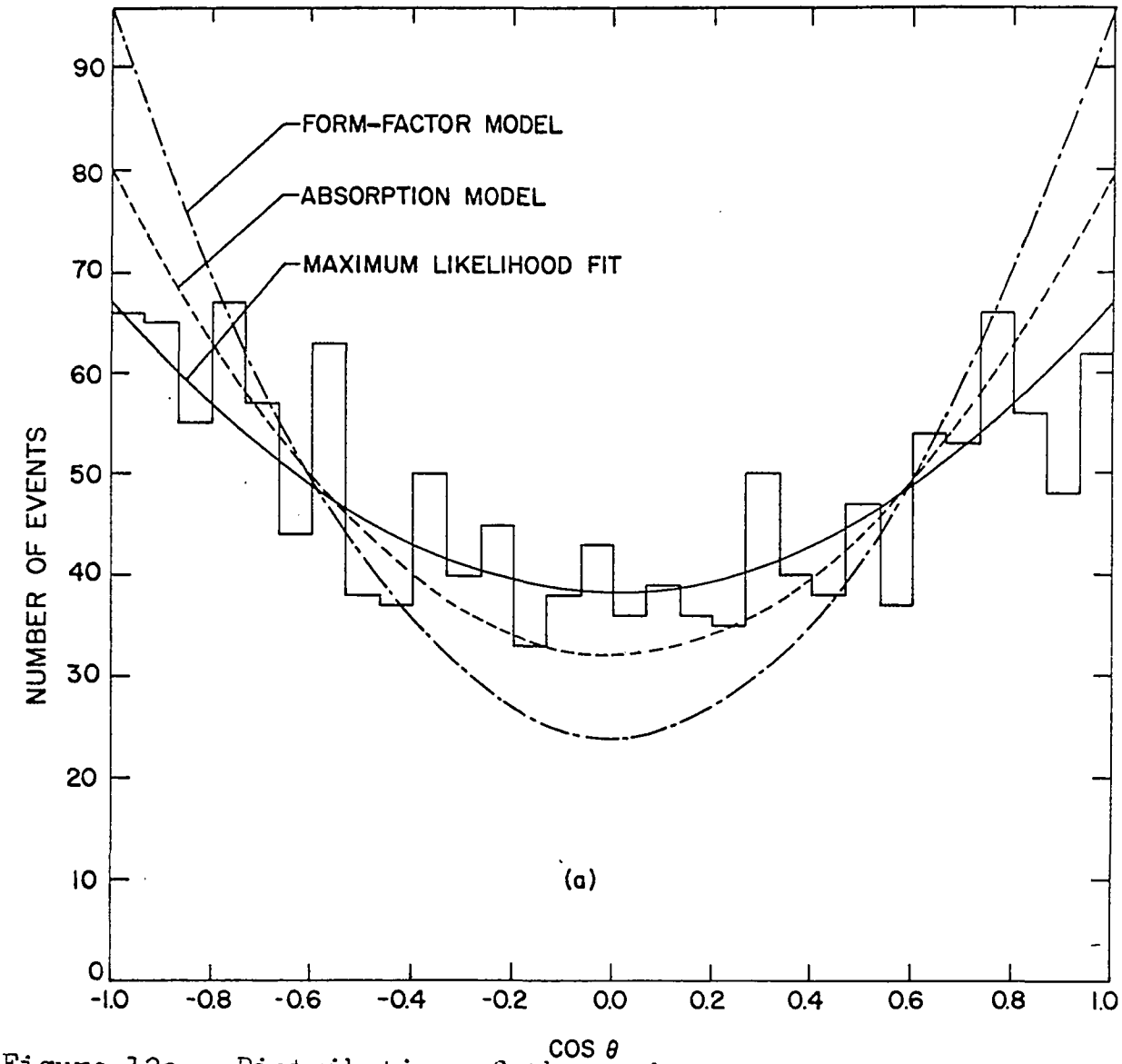

Figure 12a. Distribution of the number of events with respect to the decay angle θ, defined as the angle between the incoming $\bar{p}$ (p) and the outgoing π^- (π^+) system. Since each event occurs twice, the histogram contains 1,438 data points. The solid curve is a plot of Equation 7 using the density matrix elements obtained from a maximum likelihood fit of Equation 6 to the data. The other curves shown are the predictions of the form-factor and absorption models normalized to the data.

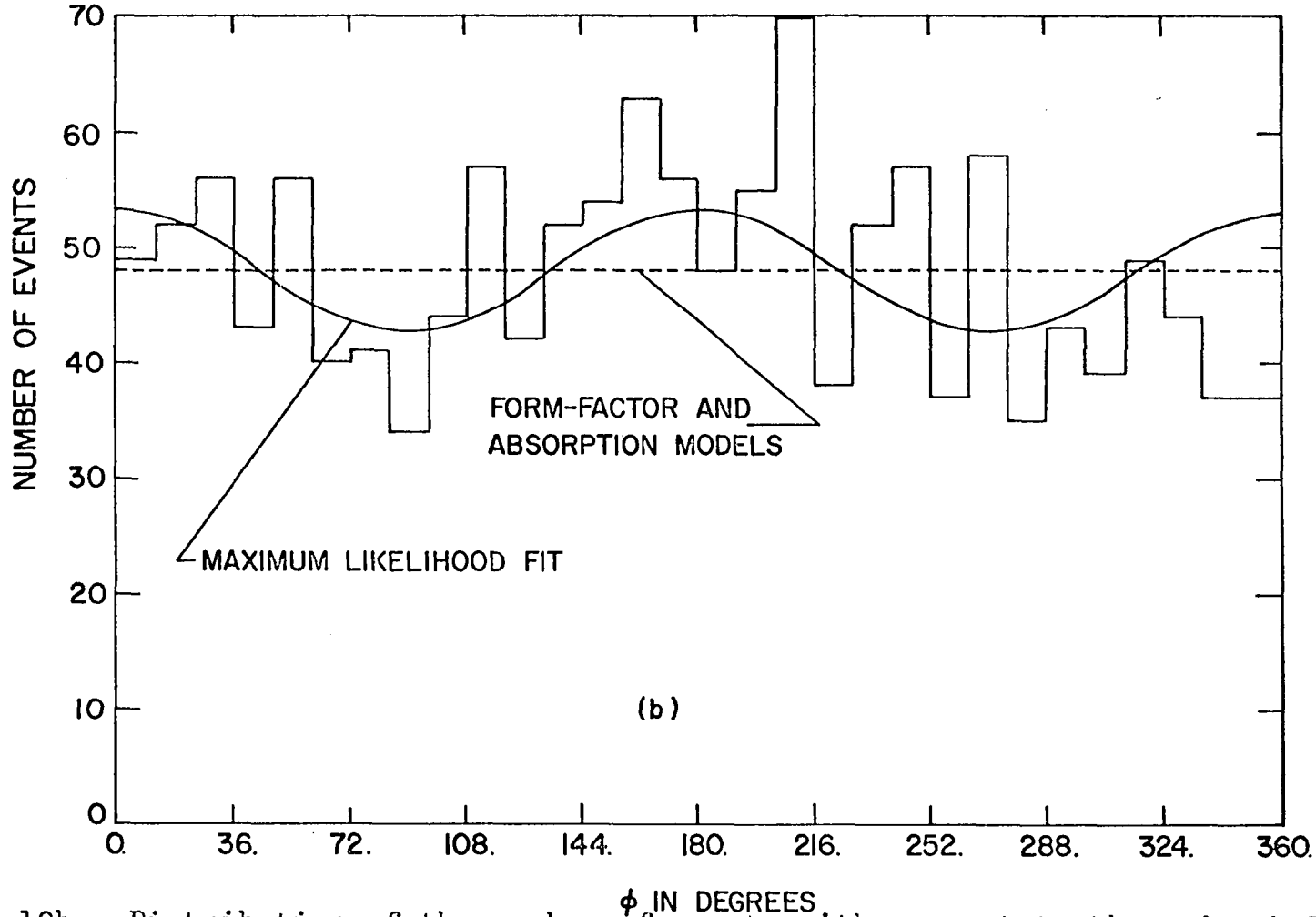

Figure 12b. Distribution of the number of events with respect to the azimuthal decay angle φ. The solid curve is a plot of Equation 8 using the density matrix elements obtained from a maximum likelihood fit of Equation 6 to the data. The dashed curve is the prediction of both the form-factor and absorption models normalized to the data.

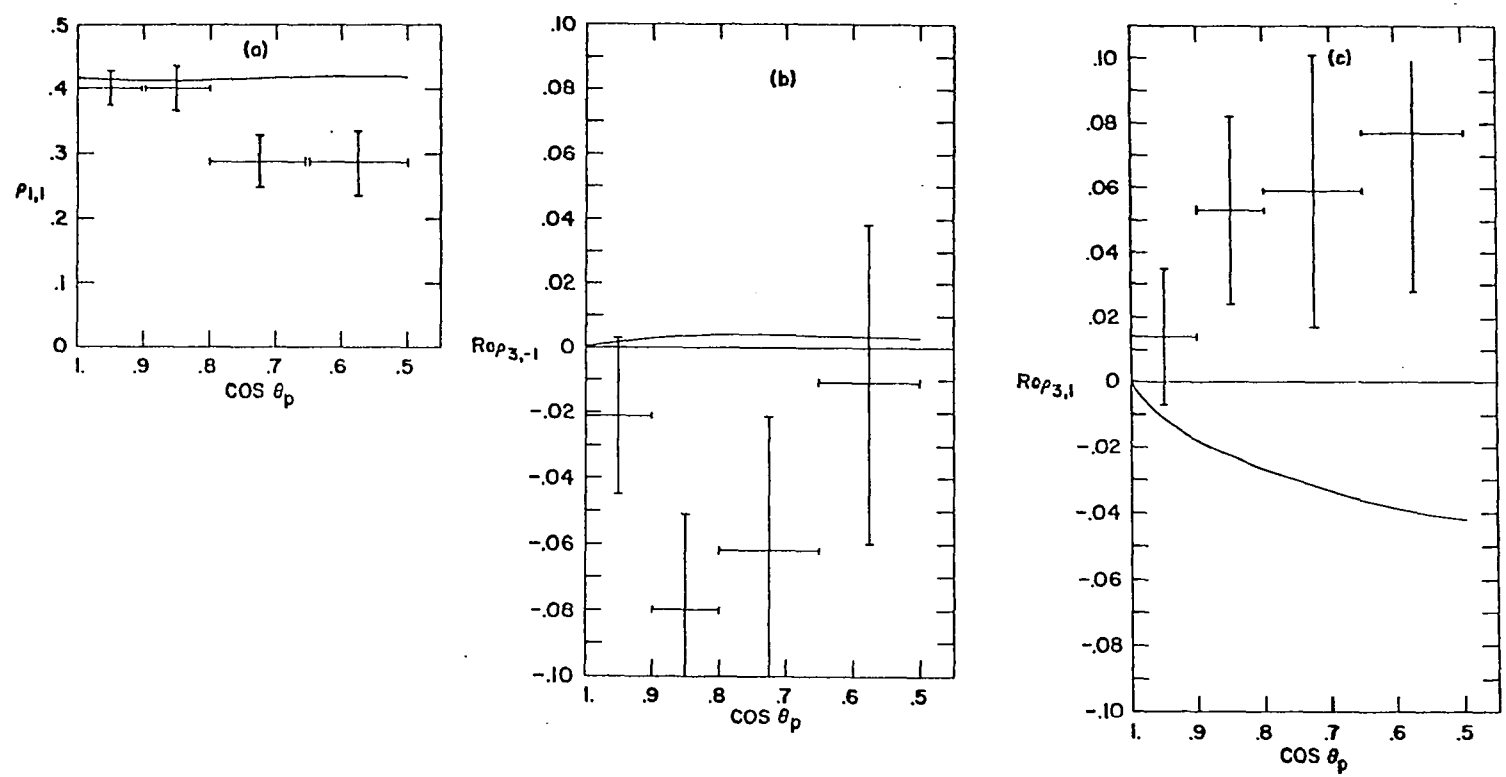

Figure 13. Density matrix elements as a function of the cosine of the production angle θ_p. The solid curves are the predictions of the absorption model.

matrix elements were fitted individually to the N* and $\bar{N}$* decay distributions. These values for the individual distributions agree with those for the combined distributions well within the assigned statistical error.

Finally, a study of the correlation in the decay of the N* with the decay of the $\bar{N}$* was made. The joint distribution of the two decay angles (θ for N* and $\bar{\theta}$ for $\bar{N}$*) is given by (24)

$$W_3(\theta,\bar{\theta}) = C_3\{[1+a(1-3\cos^2\theta)][1+a(1-3\cos^2\bar{\theta})] + b(1-3\cos^2\theta)(1-3\cos^2\bar{\theta})\} \quad (9)$$

where C_3 is a normalization constant and a and b are functions of density matrix elements. The absence of any correlation would lead to $b=0$, and the joint distribution would be simply the product of angular functions, one for the N* and one for the $\bar{N}$*. The experimental distribution was fitted to Expression 9 by a maximum likelihood calculation. The value of b that was found is $b = -0.003 \pm 0.05$, consistent with no correlation in the decays. The parameter a is related to the element $\rho_{1,1}$ and its value as determined in this analysis is consistent with that obtained using Expression 6.

IV. COMPARISON OF THE DATA WITH THE ONE-MESON-EXCHANGE MODELS

The data presented in Section III indicate the possibility of interpretation using one-pion-exchange models. Specifically, Figure 10 shows a large peak in the number of events for small production angles, that is, Reaction 1 is highly "peripheral." This peripherality suggests the presence of a long range force in the interaction, or equivalently, the exchange of a light particle. In this section the data are compared with the predictions of the form-factor and absorption models.

A. The Form-Factor Model

All possible one-pion-exchange diagrams are shown in Figure 14. In the present comparison of the predictions of the form-factor model with the data for Reaction 1 only the "double-isobar" diagram (Figure 14a) is included for reasons given below.

1. The $T_z = 1/2$ diagram

The $T_z = 1/2$ diagram is shown in Figure 14b. The contribution from a general one-pion-exchange diagram to $\bar{p}p$ scattering can be written as

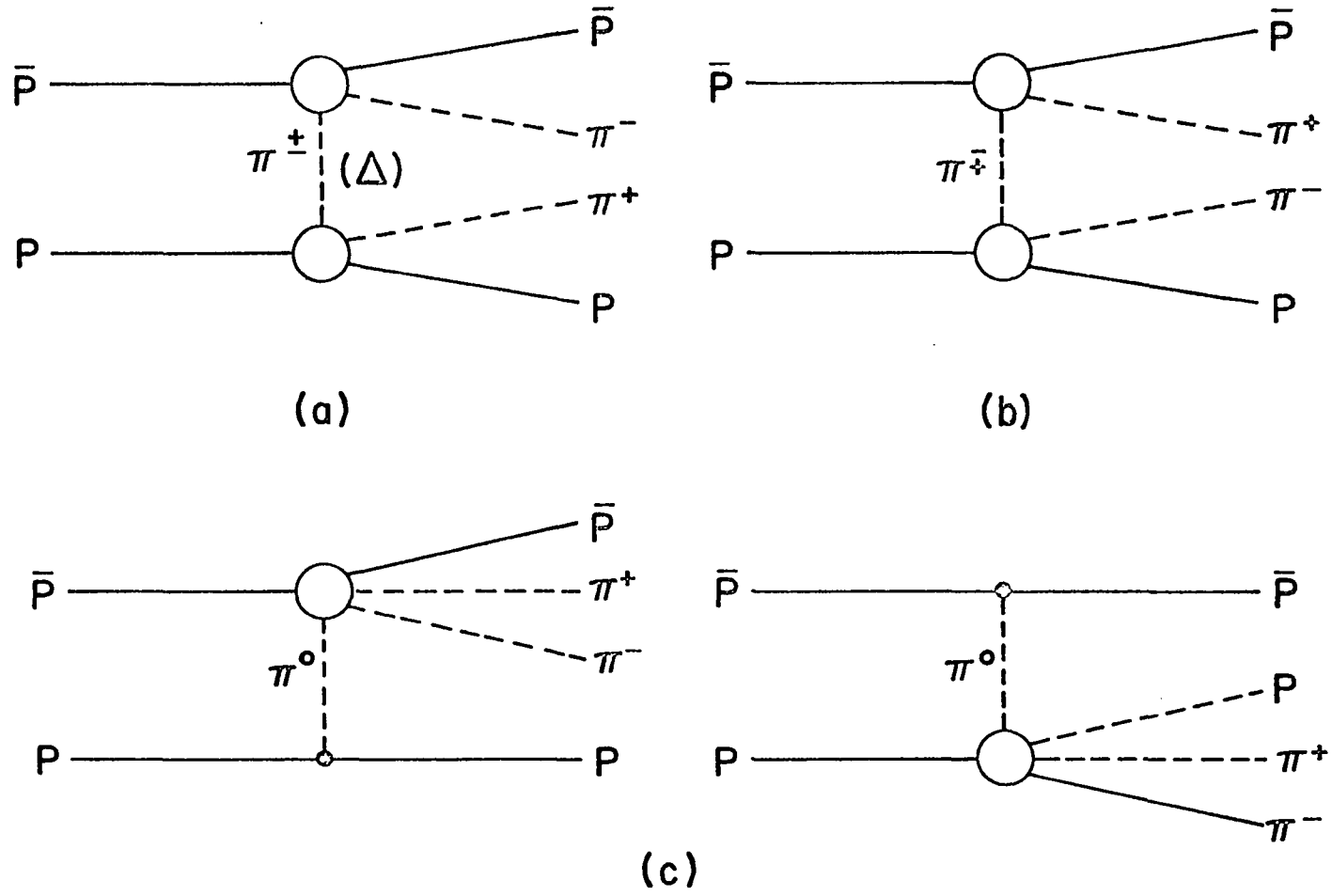

Figure 14. One-pion-exchange diagrams for the reaction $\bar{p}p \longrightarrow \bar{p}p\pi^+\pi^-$. a) Double-isobar diagram. b) $T_z = 1/2$ diagram. c) Drell diagrams.

$$\frac{d\sigma}{d\omega^2 d\bar{\omega}^2 d\Delta^2} = \Omega\, f_L\, \sigma_L(\omega)\, \frac{1}{(\Delta^2 + m^2)^2}\, f_u\, \sigma_u(\bar{\omega}) \quad (10)$$

where f_L and f_u are kinematical and dynamical factors for the lower and upper vertex, respectively, and σ_L and σ_u are the cross sections for the appropriate πN scattering process at the lower and upper vertices. Δ^2 is the square of the four-momentum transferred from the incoming nucleon to the outgoing system at the same vertex, m is the pion mass, Ω is a product of form-factors and off-shell corrections, and $(\Delta^2+m^2)^{-1}$ is the pion propagator. The invariant mass of the outgoing particles at the upper (lower) vertex $\omega\,(\bar{\omega})$ is the total center of mass energy for the scattering process at that vertex. The main difference between the $T_z = 1/2$ diagram and the double-isobar diagram in Expression 10 is in the total cross sections σ_L and σ_u. The vertex scattering processes for the $T_z = 1/2$ diagram are $\pi^- p \rightarrow \pi^- p$ and $\pi^+ \bar{p} \rightarrow \pi^+ \bar{p}$ while for the double-isobar diagram they are $\pi^+ p \rightarrow \pi^+ p$ and $\pi^- \bar{p} \rightarrow \pi^- \bar{p}$. The ratio of the cross section for $\pi^- p \rightarrow \pi^- p$ (or $\pi^+ \bar{p} \rightarrow \pi^+ \bar{p}$) to that for $\pi^+ p \rightarrow \pi^+ p$ (or $\pi^- \bar{p} \rightarrow \pi^- \bar{p}$) is 1:9. Hence the ratio of the expected contribution from the $T_z = 1/2$ diagram to that from the double-isobar diagram is 1:81. For this reason the contribution from the $T_z = 1/2$ diagram was neglected.

2. The Drell diagram

The two "Drell" diagrams are shown in Figure 14c and 14d. The contribution from the Drell diagrams is given by Ferrari (25) as

$$\frac{d\sigma}{d\omega^2 d\Delta^2} = \Lambda(\Delta^2) \frac{G^2}{4\pi W^2 p^2(\omega;M^2,m^2)} \frac{\Delta^2}{(\Delta^2+m^2)^2} \times P(\omega;M^2,m^2)\ \omega\ \sigma_0(\omega) \qquad (11)$$

where the product of form-factors and off-shell corrections Λ is

$$\Lambda(\Delta^2) = \left[1 + \frac{\Delta^2+m^2}{90\,m^2}\right]^{-2}$$

and where

$$P(\omega;M^2,m^2) = \frac{1}{2\omega}\left[\omega^4 - 2\omega^2(M^2+m^2) + (M^2-m^2)^2\right]^{\frac{1}{2}} \qquad (12)$$

$G^2 = 14.5$ is the $N^*N\pi$ coupling constant, W is the total center of mass energy, ω is the invariant mass of the final $\pi\pi N$ system, and $\sigma_0(\omega)$ is the total cross section for the process $\pi^0 p \longrightarrow \pi^+\pi^- p$ at a center of mass energy ω. This process cannot be observed directly, but the cross section was estimated by Ferrari using isotopic spin arguments and the observed cross sections of other $\pi N \longrightarrow \pi\pi N$

processes. His result was represented by a second order polynomial in ω , and Equation 11 was integrated over the allowed kinematical limits of ω and Δ^2 to determine the predicted contribution to the total cross section from the Drell diagrams. The predicted contribution is approximately 1 mb at 2.7 BeV/c. This is 62% of the contribution from the double-isobar diagram, as will be seen below. The two Drell diagrams can contribute only to non-resonance production or to single resonance production. Since the data presented in Section III are interpreted as 100% double resonance production, the contribution from the Drell diagrams was neglected on empirical grounds.

3. The double-isobar diagram

The differential cross section for Reaction 1 given by the double-isobar diagram is (12)

$$\frac{d\sigma}{d\omega^2\, d\bar{\omega}^2\, d\Delta^2} = \Omega(\omega,\bar{\omega},\Delta^2)\ \frac{1}{16\pi^3 F^2}\ \bar{\omega}\, P(\bar{\omega};M^2,m^2)$$

$$\times \sigma_1(\bar{\omega})\ \frac{1}{(\Delta^2+m^2)^2}\ \omega\, P(\omega;M^2,m^2)\ \sigma_1(\omega) \qquad (13)$$

where $M(m)$ is the nucleon (pion) mass, $\omega\ (\bar{\omega})$ is the invariant mass of the final $\pi^+p\ (\pi^-\bar{p})$ system, Δ^2 is the square of the four-momentum transfer from the incoming $\bar{p}$ to the outgoing $\pi^-\bar{p}$ system, and F^2 is a kinematical factor defined by $F^2=(P_1\cdot P_2)^2 - M^4$, where $P_2(P_1)$ is the incoming $p\ (\bar{p})$

four-momentum. $P(\omega; M^2, m^2)$ $[P(\bar{\omega}; M^2, m^2]$ is the three-momentum of the final π^+ $[\pi^-]$ in the final π^+p $[\pi^-\bar{p}]$ center of mass system and is given by Equation 12.

$\sigma_1(\omega)$ $[\sigma_1(\bar{\omega})]$ is the total cross section for the $\pi^+p \rightarrow \pi^+p$ $[\pi^-\bar{p} \rightarrow \pi^-\bar{p}]$ scattering process occurring at the lower [upper] vertex of the double-isobar diagram. For $\sigma_1(\omega)$ the Breit-Wigner form is used (26)

$$\sigma_1(\omega) = \frac{2\pi}{[P(\omega; M^2, m^2)]^2} \quad \frac{[\Gamma(\omega)]^2}{(\omega - \omega_0)^2 + [\frac{1}{2}\Gamma(\omega)]^2} \qquad (14)$$

with the empirical resonance width

$$\Gamma(\omega) = 2\gamma_\lambda^2 \frac{[P(\omega; M^2, m^2)\, a]^3}{[1 + \{P(\omega; M^2, m^2)\, a\}^2]}$$

where $2\gamma_\lambda^2 = 116$ MeV, $a = 0.88$ m^{-1}, $\omega_0 = 1237$ MeV, and $P(\omega; M^2, m^2)$ is defined by Equation 12.

The factor Ω is a product of form-factors and off-shell correction factors:

$$\Omega(\omega, \bar{\omega}, \Delta^2) = [K'(\Delta^2) \cdot K(\Delta^2) R(\omega, \Delta^2) \cdot K(\Delta^2) R(\bar{\omega}, \Delta^2)]^2. \qquad (15)$$

$K'(\Delta^2)$ is the (unknown) form-factor for the pion propagator, while $K(\Delta^2) R(\omega, \Delta^2)$ $[K(\Delta^2) R(\bar{\omega}, \Delta^2)]$ corrects the total cross section $\sigma_1(\omega)$ $[\sigma_1(\bar{\omega})]$ for the fact that

the exchanged pion is virtual. $K(\Delta^2)$ is the (unknown) form-factor for the pion-nucleon vertex. The product of unknown form-factors, K^2K' , which occurs in Equation 15 has been fitted to the $NN \rightarrow NN\pi$ data by Selleri (27) and is

$$K^2(\Delta^2)\ K'(\Delta^2) = \frac{8m^2}{\Delta^2 + 9m^2}$$

K and K' are defined such that $K(-m^2) = K'(-m^2) = 1$.
R is a known function obtained by Selleri (27), and is

$$R(\omega, \Delta^2) = \frac{f_{33}^B(\omega, \Delta^2)}{f_{33}^B(\omega, -m^2)}$$

where

$$f_{33}^B(\omega, \Delta^2) = \alpha(\omega)\left[\frac{\omega - M}{R_-} Q_1(\beta) - \frac{\omega + M}{R_+} Q_2(\beta)\right]$$

$$R_\pm = \left[(p_{10} \pm M)(p_{20} \pm M)\right]^{1/2}$$

$$Q_1(\beta) = \frac{\beta}{2} \log\frac{\beta+1}{\beta-1} - 1$$

$$Q_2(\beta) = \frac{3\beta^2-1}{4} \log\frac{\beta+1}{\beta-1} - \frac{3}{2}\beta$$

$$\beta = \frac{2p_{10}(\omega - p_{20}) - m^2}{2R_+R_-}$$

$$p_{10} = \frac{\omega^2 + M^2 + \Delta^2}{2\omega}$$

$$p_{20} = \frac{\omega^2 + M^2 - m^2}{2\omega} \quad .$$

The function $R(\omega, \Delta^2)$ is valid only in the "3,3 resonance region," but because of the low total center of mass energy in the present experiment the full range of ω ($\overline{\omega}$) is included in this region.

Since Ω and σ_1 are completely determined by previous experiments, Equation 1 contains no undetermined parameters.

4. Comparison with the data

The predictions of the form-factor model from Equation 13 for the present experiment are shown in Figures 12, 15, and 16 where all theoretical curves are normalized to the data. The theoretical differential cross section with respect to the square of the four-momentum transfer from the initial $\overline{p}$ to the final $\pi^-\overline{p}$ system is compared with the data in Figure 15. The theoretical curve is too sharply peaked and falls off too rapidly at higher momentum transfers, but as a whole is in fair agreement with the histogram. The shape of the theoretical curve would be slightly improved by including the contribution from the Drell diagrams, but, as mentioned above, this is not consistent with the observed 100% double isobar production. The invariant mass distribution of the final π^+p and

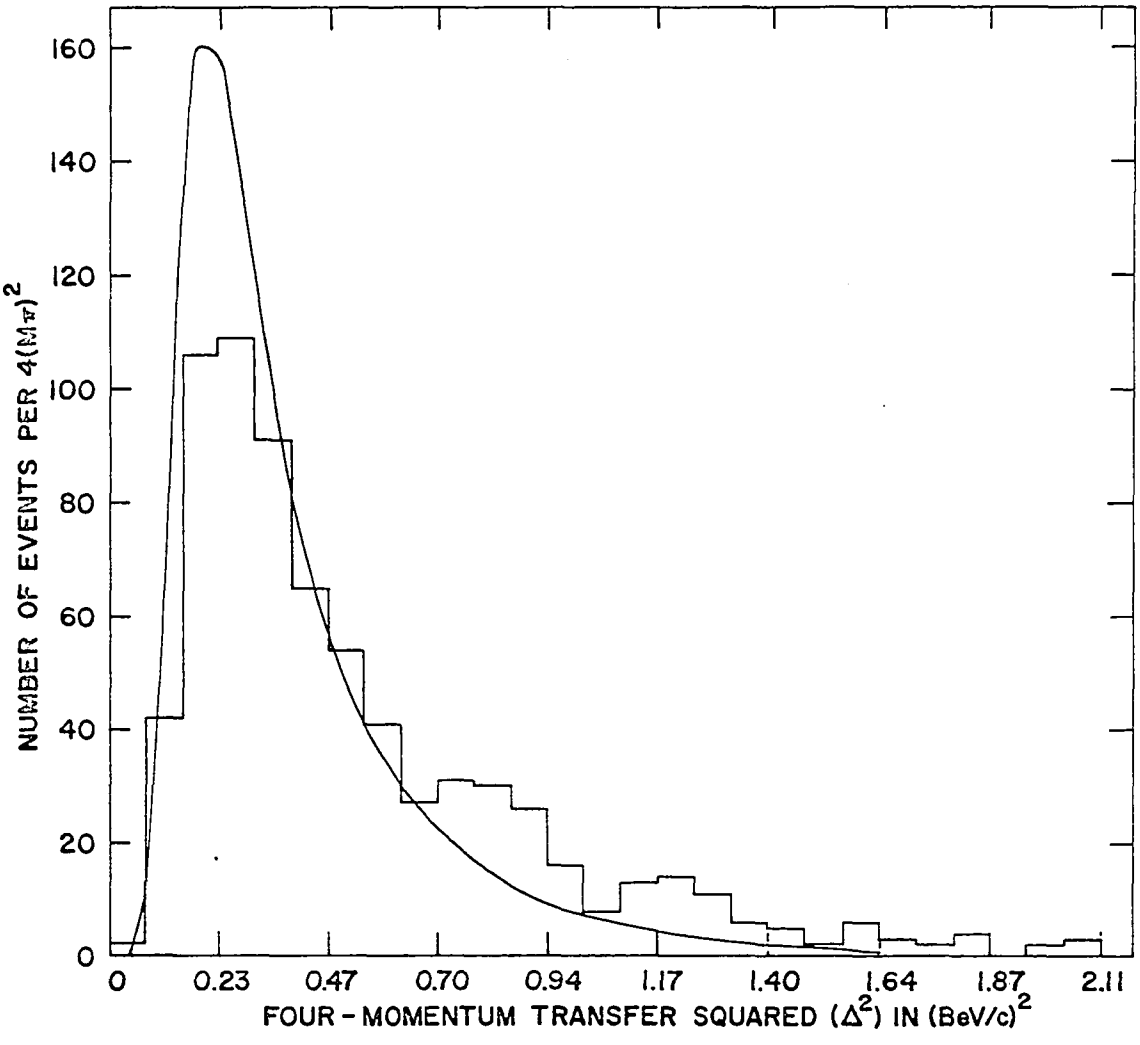

Figure 15. Differential cross section with respect to the square of the four-momentum transfer from the incident $\bar{p}$ to the final $\pi^-\bar{p}$ system. The histogram is based on 719 events. The solid curve is the prediction of the form-factor model calculated from Equation 13. The theoretical curve is normalized to the data.

$\pi^-\bar{p}$ systems predicted by the form-factor model is compared with the data in Figure 16. (The π^+p and $\pi^-\bar{p}$ invariant mass histograms are combined.) The empirical Breit-Wigner resonance forms, Equation 14, have a peak at 1225 MeV. The effect of the form-factors and off-shell correction factors of Equation 15 is to bring the peak of the predicted invariant mass distribution down to 1218 MeV so that the theoretical curve is in good agreement with the data.

The form-factor model for Reaction 1, as based on the double-isobar diagram, assumes the dominance of one diagram with the exchange of a spinless particle and no final state interactions. The π N relative orbital angular momentum ($\ell = 1$) is perpendicular to the z axis (Figure 11) so that the only possible spin projections along the z axis are $m = \pm 1/2$. Hence, the only non-vanishing amplitudes are those with these spin projections. Therefore, under the assumption of no final state interactions only $\rho_{1,1}$ can be non-zero, and the prediction for the density matrix elements is (15) $\rho_{1,1} = 1/2$ and $\rho_{3,1} = \rho_{3,-1} = 0$. This may be compared with the experimentally determined values given in Section III. Thus the distribution $W_1(\theta)$ has the simple form $1 + 3\cos^2\theta$, while $W_2(\varphi)$ is independent of the azimuthal decay angle φ, that is, the distribution in φ is predicted to be isotropic. (This result for W_1 and W_2 is, of course, the decay distribution observed for a "free" N*.) In Figure 12a the $1+3\cos^2\theta$ form for $W_1(\theta)$ (labeled form-factor model) is compared with

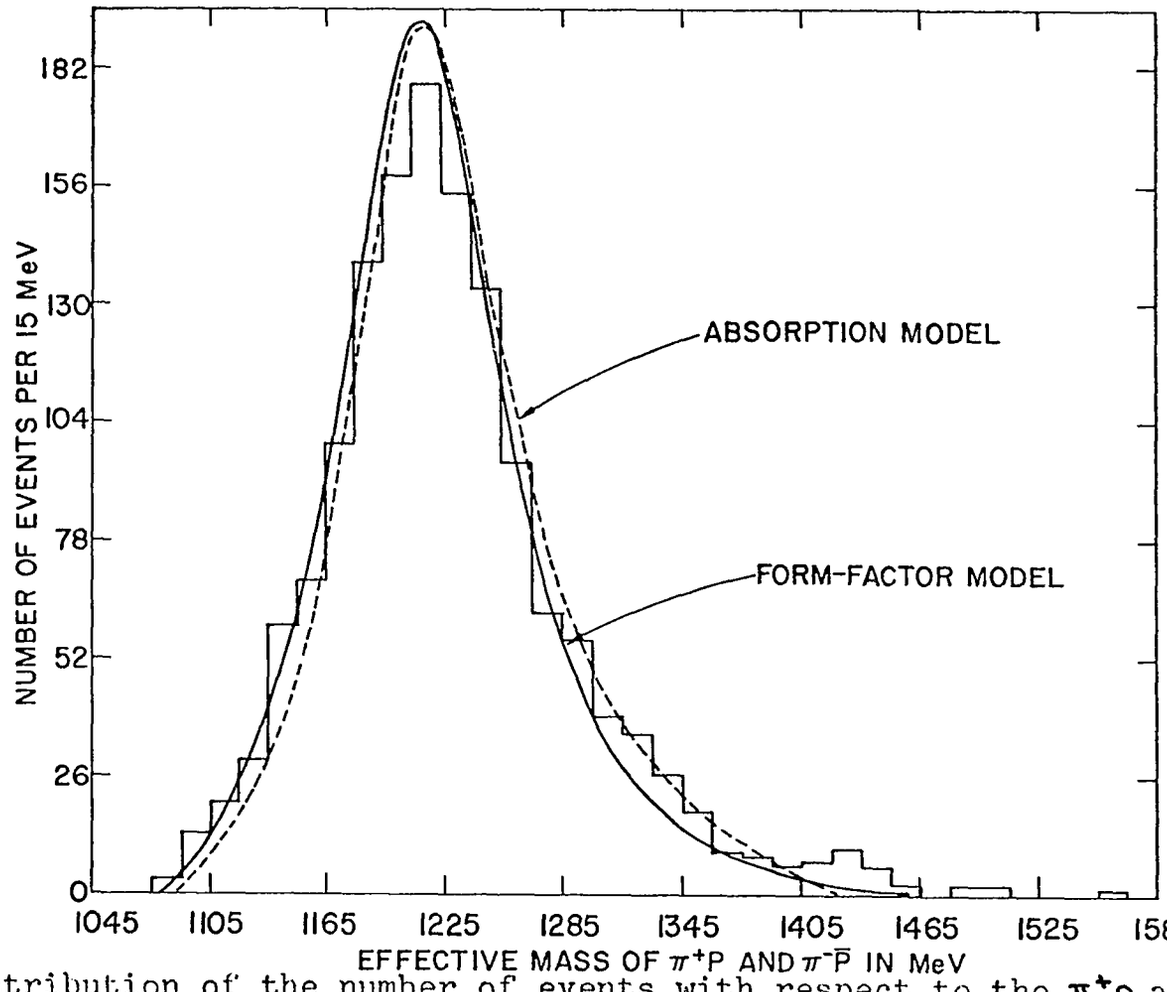

Figure 16. Distribution of the number of events with respect to the π^+p and $\pi^-\bar{p}$ effective masses (1, 438 data points). The solid curve is the prediction of the form-factor model calculated from Equation 13. The dashed curve is the prediction of the absorption model. Both theoretical curves are normalized to the data.

the data. The agreement is seen to be poor. In Figure 12b the theoretical distribution $W_2(\varphi)$, predicted isotropic in φ, is represented by a straight line. As pointed out in Section III the experimental distribution is not isotropic.

The form-factor model based only on the double-isobar diagram predicts a total cross section for Reaction 1 at 2.7 BeV/c of 1.62 mb which is in good agreement with the experimental value of 1.93 ± 0.16 mb.

5. Remarks on the Drell diagrams

The inclusion of the Drell diagrams in the predictions of the form-factor model would

1) raise the predicted cross section to 2.6 mb,
2) reduce the sharpness of the peak of the $d\sigma/d\Delta^2$ distribution, but would make the distribution too large for $\Delta^2 \gtrsim 0.4$ $(\text{BeV/c})^2$, and
3) completely destroy the agreement between the predicted curve and the histogram for the invariant π^+p ($\pi^-\bar{p}$) mass distribution.

B. The Absorption Model

1. The calculation

Hite and Jackson* have calculated the absorption model

*G. E. Hite and J. D. Jackson, Department of Physics, University of Illinois, Urbana, Illinois. Absorption Model for $\bar{p}p \longrightarrow N^*\bar{N}^*$ at 2.7 BeV/c. Private Communication. 1966.

predictions for the reaction $\bar{p}p \rightarrow N^*\bar{N}^*$. The essentials of their calculation are:

a) an exact summation of the series of modified partial wave amplitudes is performed instead of approximating the sum by an integral over an impact parameter as is usually done (16);

b) the absorption parameters in the initial ($\bar{p}p$) and final ($N^*\bar{N}^*$) states are $\gamma_1 = 0.03$, $C_1 = 1.0$, and $\gamma_2 = 0.01$, $C_2 = 1.0$, respectively (in the notation of (16). These absorption parameters are chosen, within the freedom allowed by the errors in the $\bar{p}p$ elastic scattering data, to improve the predictions of the absorption model for the present experiment, particularly to improve the fit to the differential cross section $d\sigma/d(\cos\theta_p)$ and to the total cross section;

c) the $N^*N\pi$ coupling constant used is $G^{*2}/4\pi = 0.428$ (in the notation of (28)); and

d) the calculated differential cross section for the production of the two "stable" isobars is multiplied by two Breit-Wigner resonance expressions to include the effects of the resonance decays. The resonance expressions are of the type discussed by Jackson (21) with the usual P-wave resonance width modified to include about 10% S-wave. The value of ω_o was chosen as 1230 MeV instead of the usual 1237 MeV. These two modifications are made to improve the absorption model

prediction of the invariant mass distribution for the present experiment.

2. Comparison with the data

The predictions of the absorption model calculation of Hite and Jackson are shown in Figures 10, 12, 13, and 16 where the theoretical curves are normalized to the data. The theoretical curve and the histogram for the differential cross section with respect to the production angle are shown in Figure 10. The agreement is good, but the theoretical curve is not peaked as strongly at small angles as the data. The theoretical curve and the data for the invariant mass distribution of the final isobars are shown in Figure 16. The agreement is good.

Although the absorption model calculation for $\bar{p}p \rightarrow N^*\bar{N}^*$ involves the dominance of a single diagram with the exchange of a spinless particle, the inclusion of initial and final state interactions means that the density matrix elements predicted by the absorption model will differ from those predicted by the form-factor model. The theoretical and experimental density matrix elements as a function of the production angle are shown in Figure 13. The theoretical and experimental values of $\rho_{1,1}$ agree at small production angles, but diverge with increasing production angle. For Re $\rho_{3,1}$ and Re $\rho_{3,-1}$ the theoretical predictions are inconsistent with the data. The absorption model prediction for the decay distribution $W_1(\theta)$ is shown with the data in Figure 12a. The agree-

ment is adequate. The theoretical decay distribution $W_2(\varphi)$ predicted by the absorption model is shown as a straight line in Figure 12b because the predicted value of Re $\rho_{3,-1}$ is too small to produce a detectable deviation from isotropy. As remarked in Section III the observed distribution is not isotropic.

The absorption model predicts a total cross section of 2.2 mb for $\cos\theta_p \geq 0.5$. This is to be compared with an experimental cross section of 1.4 mb for events with this restriction.

V. CONCLUSION

This reaction $\bar{p}p \rightarrow \bar{p}p\pi^+\pi^-$ has been studied over a wide range of incident $\bar{p}$ momenta. The total cross section at six energies is given in Table 1. The cross section rises slowly from the double pion production threshold of 1.2 BeV/c, but rapidly from the double N*(1238) threshold of 2.0 BeV/c, remaining relatively constant for higher beam momenta. These facts reflect the importance of N* formation in Reaction 1. Also shown in Table 1 are estimates of the amounts of zero, single, and double resonance production. Near threshold Reaction 1 appears to be dominated by double N* formation, while substantial fractions of single and zero resonance production occur at higher energies.

The second outstanding characteristic of the data at all energies is that the differential cross section with respect to the square of the four-momentum transfer from the initial $\bar{p}$ to the final $\pi^-\bar{p}$ system ($d\sigma/d\Delta^2$) is sharply peaked at small Δ^2. The shape of the peak does not change appreciably with energy, however larger fractions of events with high four-momentum transfer occur as the energy is increased.

In the present paper the density matrix elements are given as a function of production angle θ_p at 2.7 BeV/c. Svensson (29) gives the density matrix elements as a function of the square of the four-momentum transfer Δ^2 at 3.6 and 5.7 BeV/c. A comparison of Figure 13a and Svensson's results

Table 1. Total cross sections for the reaction $\bar{p}p \longrightarrow \bar{p}p\pi^+\pi^-$

Incident $\bar{p}$ lab momentum (BeV/c)	Total cross section $\bar{p}p \xrightarrow{(mb)} \bar{p}p\pi^+\pi^-$	Fraction of N*(1238) production (%)			Reference
		zero ($\pi^+p\pi^-\bar{p}$)	single ($N^*\pi^-\bar{p}$ and $\pi^+p\bar{N}^*$)	double ($N^*\bar{N}^*$)	
2.7	1.93 ± 0.16	0	0	100	present paper
3.28	3.43 ± 0.23	-	-	80	5
3.6	3.80 ± 0.22	-	-	56	6
3.66	3.67 ± 0.30	-	-	50-80[a]	7
5.7	3.18 ± 0.16	20	50	30	8
5.7	3.31 ± 0.16	16	21	63	9
6.94	3.0 ± 0.7	-	-	50	10

[a]The 50% figure is obtained from a comparison of the form-factor model (including Drell diagrams) with the data. The 80% figure is obtained by fitting the invariant π^+p ($\pi^-\bar{p}$) mass distribution with phase space and S-wave Breit-Wigner shapes with peaks at 1215 MeV and $\Gamma = 90$ MeV.

shows that $\rho_{1,1}$ does not vary in magnitude or in Δ^2 dependence as the incident $\bar{p}$ momentum is changed. This means that the $\cos\theta$ decay distribution does not change appreciably with energy. In contrast to this, the values of Re $\rho_{3,-1}$ and Re $\rho_{3,1}$ vary considerably with energy. At 2.7 BeV/c the value of Re $\rho_{3,-1}$ is four standard deviations from zero, and the φ decay distribution is anisotropic. At higher energies the decay distribution is observed to be isotropic, and the values of Re $\rho_{3,-1}$ are consistent with zero. The density matrix element Re $\rho_{3,1}$ has small positive values at 2.7 BeV/c, values consistent with zero at 3.6 BeV/c, and small negative values at 5.7 BeV/c. No correlation between the θ decay angles for the N* and the $\bar{N}$* is observed at 2.7 BeV/c, while a small correlation is observed at higher beam momenta.

It is not possible to make a detailed comparison of the form-factor and absorption model predictions made in this paper with those made for the other experiments listed in Table I because of the following differences. The differences between the present and previous applications of the form-factor model are:

1) the form-factors and off-shell corrections used in the present calculation are those of Selleri (27), while the previous calculations (6-10) used the result of Ferrari and Selleri (30); and
2) the present calculation includes only the contribution of the double-isobar diagram, while the previous com-

parisons also include the Drell and $T_{\pi} = 1/2$ diagrams.

For the absorption model, the present calculation of Hite and Jackson differs from the calculation of Svensson (29) in that:

1) in the present calculation the series of modified partial wave amplitudes is summed exactly while Svensson uses a Bessel function approximation for the partial wave amplitudes and approximates the series by an integral; and
2) Hite and Jackson include Breit-Wigner resonance shapes to incorporate the effects of the N* and $\bar{N}$* decays, while Svensson does not.

VI. BIBLIOGRAPHY

1. W. J. Kernan, D. E. Lyon, and H. B. Crawley, Phys. Rev. Letters 15, 803 (1965).

2. D. E. Bohning and W. J. Kernan, (Abstract) Bull. Am. Phys. Soc. 10, 1115 (1965).

3. L. S. Schroeder, D. E. Bohning, W. J. Kernan, V. Domingo, Å. Eide, G. Fisher, R. Sears, and J. Von Krogh, (Abstract) Bull. Am. Phys. Soc. 11, 360 (1966).

4. W. J. Kernan, D. E. Bohning, L. S. Schroeder, V. Domingo, Å. Eide, G. Fisher, R. Sears, and J. Von Krogh, (Abstract) Bull. Am. Phys. Soc. 11, 360 (1966).

5. T. Ferbel, J. Sandweiss, H. D. Taft, M. Gailloud, T. E. Kalogeropoulos, T. W. Morris, and R. M. Lea, Phys. Rev. Letters 9, 351 (1962)

6. H. C. Dehne, E. Lohrmann, E. Raubold, P. Söding, M. W. Teucher, and G. Wolf, Phys. Rev. 136, B843 (1964).

7. T. Ferbel, A. Firestone, J. Sandweiss, H. D. Taft, M. Gailloud, T. W. Morris, W. J. Willis, A. H. Bachman, P. Baumel, and R. M. Lea, Phys. Rev. 138, B1528 (1965).

8. K. Böckmann, B. Nellen, E. Paul, B. Wagini, I. Borecka, J. Diaz, U. Heeren, U. Liebermeister, E. Lohrmann, E. Raubold, P. Söding, S. S. Wolff, J. Kidd, L. Mandelli, L. Mosca, V. Pelosi, S. Ratti, and L. Tallone, Nuovo Cimento 42, 954 (1966).

9. V. Alles-Borelli, B. French, A. Frisk, and L. Michedja, CERN [European Council for Nuclear Research] Preprint CERN/TC/Physics 66-10, (1966).

10. T. Ferbel, A. Firestone, J. Johnson, J. Sandweiss, and H. D. Taft, Nuovo Cimento 38, 19 (1965).

11. A. C. Hearn and S. D. Drell, Stanford University Report SLAC/PUB 176, 1 (1966).

12. E. Ferrari and F. Selleri, Suppl. Nuovo Cimento 24, 453 (1962).

13. N. J. Sopkovich, Nuovo Cimento 26, 186 (1962).

14. L. Durand III and Y. T. Chiu, Phys. Rev. 139, B646 (1965).

15. K. Gottfried and J. D. Jackson, Nuovo Cimento 34, 735 (1964).

16. J. D. Jackson, Rev. Mod. Phys. 37, 484 (1965).

17. F. Selleri, Nuovo Cimento 42, 835 (1966).

18. C. Baltay, J. Sandweiss, J. Sanford, H. Brown, M. Webster, and S. Yamamoto, Brookhaven National Laboratory Report BNL 6212, 1 (1962).

19. J. P. Berge, F. T. Solmitz, and H. D. Taft, Rev. Sci. Instr. 32, 538 (1961).

20. A. Pais, Phys. Rev. Letters 3, 242 (1959).

21. J. D. Jackson, Nuovo Cimento 34, 1644 (1964).

22. R. J. Pankhurst, GERN [European Council for Nuclear Research] Program Library [Publication] D 502, 1 (1964).

23. K. Gottfried and J. D. Jackson, Nuovo Cimento 33, 309 (1965).

24. H. Pilkuhn and B. E. Y. Svensson, Nuovo Cimento 38, 518 (1965).

25. E. Ferrari, Nuovo Cimento 30, 240 (1963).

26. M. Gell-Mann and K. M. Watson, Ann. Rev. Nucl. Sci. 4, 219 (1954).

27. F. Selleri, Nuovo Cimento 40, 236 (1965).

28. J. D. Jackson and H. Pilkuhn, Nuovo Cimento 33, 906 (1964).

29. B. E. Y. Svensson, Nuovo Cimento 39, 667 (1965).

30. E. Ferrari and F. Selleri, Nuovo Cimento 27, 1450 (1963).

31. Lyman G. Parratt, Probability and Experimental Errors in Science (John Wiley and Sons, Inc., New York, 1961).

VII. ACKNOWLEDGEMENTS

The author wishes to express his sincere gratitude to Professor W. J. Kernan for his personal interest and guidance throughout the course of this investigation. He also wishes to thank Dr. R. A. Leacock for his invaluable help in the theoretical interpretation of the data and for many discussions concerning other phases of this problem.

Appreciation is expressed to the scanning and measuring staff of Experimental Physics Group XII. This includes Miss Andrea Carlisle, Mrs. Marlene Frisk, Mrs. Juanita Lincoln, Mrs. Betty Pepper, Mrs. Jean Rostenbach, Mrs. Joyce Tonne, and Mrs. Rita Wagstaff. Without their many hours of diligent work in the scanning and measuring of the bubble chamber film this work would not have been possible. Much credit is also due to the programming staff under Mr. W. J. Higby.

Acknowledgement is given to Professor J. D. Jackson and Mr. G. E. Hite for the results of their absorption model calculation and for helpful discussions.

The author would like to express his appreciation for the financial support given to him during his graduate studies: to the Iowa State University Research Foundation for the year 1962-63; to the National Science Foundation for the year 1963-64; and to the National Aeronautics and Space Administration for the remaining two years 1964-66.

Finally, a great deal of credit is due the author's wife

for her understanding and support throughout his graduate work and for her help in the typing of this manuscript.

VIII. APPENDIX A

The method of maximum likelihood is a general method for obtaining the best statistical fit of a set of measurements of independent variables, say $x_1, x_2, \cdots, x_n$, to a known function of these independent variables and a number of parameters, say $\gamma_1, \gamma_2, \cdots, \gamma_m$. If $F(x_1, x_2, \cdots, x_n ; \gamma_1, \gamma_2, \cdots \gamma_m)$ is this known function then the likelihood function is defined as (31, p. 103)

$$L(x_1, x_2, \cdots, x_n ; \gamma_1, \gamma_2, \cdots, \gamma_m) = \prod_{i=1}^{N} F(x_1^i, x_2^i, \cdots, x_n^i ; \gamma_1, \gamma_2, \cdots, \gamma_m)$$

where $x_1^i, x_2^i, \cdots, x_n^i$ are the measured values and the product contains the total number, N, of measurements of the variables. In the limit of $N \longrightarrow \infty$ the likelihood function approaches a normal distribution as a function of the parameters γ, and the best fit is obtained with the values of γ which maximize the likelihood function. The usual procedure for finding this maximum is to maximize the logarithm of the likelihood function with respect to the parameters; that is, to satisfy the m simultaneous equations

$$\frac{\partial \log L}{\partial \gamma_j} = 0 = \sum_{i=1}^{N} \frac{\partial}{\partial \gamma_j} \log F(x_1^i, x_2^i, \cdots, x_n^i ; \gamma_1, \cdots, \gamma_j, \cdots \gamma_m)$$

This procedure was used in all maximum likelihood calculations in this dissertation.

IX. APPENDIX B

An alternative method has been used in the literature (8, 9) to evaluate the density matrix elements. This procedure consists of taking the average value of certain trigonometric functions. In particular these relations can be used

$$\rho_{1,1} = \frac{15}{8} \langle \cos^2\theta \rangle - \frac{3}{8}$$

$$\mathrm{Re}\,\rho_{3,1} = -\frac{5\sqrt{3}}{8} \langle \sin 2\theta \cos\varphi \rangle$$

$$\mathrm{Re}\,\rho_{3,-1} = -\frac{\sqrt{3}}{2} \langle \cos 2\varphi \rangle .$$

Experimentally the average value of a function, for example $\langle \cos^2\theta \rangle$, is defined as

$$\langle \cos^2\theta \rangle = \frac{1}{N} \sum_{i=1}^{N} \cos^2\theta_i$$

where N is the number of experimental data points. Then the error in $\langle \cos^2\theta \rangle$ is

$$\delta\langle \cos^2\theta \rangle = \left\{ \frac{1}{N} \sum_{i=1}^{N} \left[\cos^2\theta_i - \langle \cos^2\theta \rangle \right]^2 \right\}^{1/2} .$$

This procedure was used to evaluate the density matrix elements $\rho_{1,1}$, Re $\rho_{3,1}$, and Re $\rho_{3,-1}$ averaged over production angle and using the combined N* and $\bar{N}$* data. The result is $\rho_{1,1} = 0.348 \pm 0.015$, Re $\rho_{3,-1} = -0.039 \pm 0.016$ and Re $\rho_{3,1} = -0.002 \pm 0.0156$. Comparing with the values obtained by the maximum likelihood procedure given in Section III, the values of $\rho_{1,1}$ and Re $\rho_{3,-1}$ agree within the statistical errors. However, the values of the θ-φ correlation parameter Re $\rho_{3,1}$ determined by the two procedures do not agree. It is felt that the values obtained by the maximum likelihood procedure are more valid for purposes of comparing with the predictions of the absorption model, since these values do give the best fit to the assumed θ-φ distribution. The disagreement in the values of Re $\rho_{3,1}$ may reflect an additional type of θ-φ correlation which is not included in the general form for $W(\theta,\varphi)$.